

# Mean-field study of hot $\beta$ -stable protoneutron star matter: Impact of the symmetry energy and nucleon effective mass

Ngo Hai Tan<sup>1,2</sup>, Doan Thi Loan<sup>1</sup>, Dao T. Khoa<sup>1,\*</sup> and Jerome Margueron<sup>2</sup>

<sup>1</sup> *Institute for Nuclear Science and Technology, VINATOM  
179 Hoang Quoc Viet, Cau Giay, Hanoi, Vietnam.*

<sup>2</sup> *Institut de Physique Nucléaire de Lyon, IN2P3-CNRS  
4 Rue Enrico Fermi, 69622 Villeurbanne Cedex, France.*

(Dated: March 10, 2016)

## Abstract

A consistent Hartree-Fock study of the equation of state (EOS) of asymmetric nuclear matter at finite temperature has been performed using realistic choices of the effective, density dependent nucleon-nucleon (NN) interaction, which were successfully used in different nuclear structure and reaction studies. Given the importance of the nuclear symmetry energy in the neutron star formation, EOS's associated with different behaviors of the symmetry energy were used to study hot asymmetric nuclear matter. The slope of the symmetry energy and nucleon effective mass with increasing baryon density was found to affect the thermal properties of nuclear matter significantly. Different density dependent NN interactions were further used to study the EOS of hot protoneutron star (PNS) matter of the  $npe\mu\nu$  composition in  $\beta$ -equilibrium. The hydrostatic configurations of PNS in terms of the maximal gravitational mass  $M_{\text{max}}$  and radius, central density, pressure and temperature at the total entropy per baryon  $S/A = 1, 2$  and  $4$  have been determined in both the neutrino-free and neutrino-trapped scenarios. The obtained results show consistently a strong impact of the symmetry energy and nucleon effective mass on thermal properties and composition of hot PNS matter.  $M_{\text{max}}$  values obtained for the (neutrino-free)  $\beta$ -stable PNS at  $S/A = 4$  were used to assess time  $t_{\text{BH}}$  of the collapse of  $40 M_{\odot}$  protoneutron progenitor to black hole, based on a correlation between  $t_{\text{BH}}$  and  $M_{\text{max}}$  found from the hydrodynamic simulation by Hempel *et al.*

PACS numbers: 21.65.Cd; 25.65.Ef; 21.65.Mn; 26.60.Kp

---

\*Electronic address: khoa@vinatom.gov.vn

## I. INTRODUCTION

A realistic equation of state (EOS) of asymmetric nuclear matter (NM) is the most vital input for the study of the neutron star formation [1–6], and the determination of the EOS has been, therefore, the focus of many nuclear structure and reaction studies involving exotic nuclei lying close to the driplines. The key quantity to distinguish the different nuclear EOS's is the nuclear mean-field potential that can be obtained from a consistent mean-field study, like the relativistic mean-field (RMF) [7] or Hartree-Fock (HF) [8] calculations of NM using the realistic interaction between nucleons in the high-density nuclear medium. As such, the different nuclear EOS's have been used in the hydrodynamic simulation of core-collapse supernovae [9, 10] to study the hot protoneutron star (PNS) formed in the aftermath of supernovae [11–13] and its collapse to black hole or evolution towards cold neutron star. The latter is an extensive research object of numerous nuclear many-body studies (see, e.g., Refs. [8, 14–16, 18, 19]).

The microscopic many-body studies, like the Brueckner-Hartree-Fock (BHF) calculations [12, 16, 17], have shown the important role played by the Pauli blocking effects as well as the higher-order nucleon-nucleon (NN) correlations at large NM densities. Such medium effects serve as the physics origin of the empirical density dependence introduced into various versions of the effective NN interactions being widely used in the nuclear structure and reaction studies. Quite popular are the density dependent versions of the M3Y interaction (originally constructed in terms of three Yukawas to reproduce the G-matrix elements of the Reid [20] and Paris [21] NN potentials in an oscillator basis), which have been applied successfully in the folding model studies of nuclear scattering [22–25] or in the HF structure calculations of finite nuclei [26–28]. The different versions of the density dependent M3Y interaction have been used recently, together with the D1S and D1N versions of Gogny interaction [29, 30] and SLy4 version [32] of Skyrme interaction [31], to study the basic properties of asymmetric NM at zero temperature [19] as well as the  $\beta$ -stable matter of cold neutron star [8]. While all these interactions give about the same description of the saturation properties of symmetric NM, the HF results for asymmetric NM [19] show that they are roughly divided into two groups that are associated with two different (so-called *soft* and *stiff*) behaviors of the nuclear symmetry energy at high NM densities. In the soft scenario, the symmetry energy changes its slope and decreases at high NM densities,

resulting on a drastic decrease of the proton and lepton components in the core of neutron star that then becomes  $\beta$ -unstable. A very small proton fraction in neutron star matter given by the soft-type mean-field potentials excludes the direct Urca (DU) process in the neutron star cooling, whereas the DU process is well possible in the  $\beta$ -equilibrated neutron star matter predicted by the stiff-type mean field potentials [8]. A vital role of the nuclear symmetry energy has also been illustrated with the density dependent M3Y interaction, where a significant reduction of the maximum gravitational mass and radius of neutron star was found when the slope of the symmetry energy was changed from the stiff behavior to the soft one [8].

Because the composition and physical conditions of a hot newly born PNS are quite different from those of a cold and lepton-poor neutron star, it is of high interest to extend the mean-field approach of Ref. [8] to the study of the hot baryon matter of PNS, and explore the sensitivity of the PNS composition to the nuclear symmetry energy at finite temperature and entropy as well as the effects caused by neutrino trapping. For this purpose, the reliability of the present HF approach was tested first in the mean-field study of hot and dense asymmetric NM, and the results are presented in Sec. II. These results turn out to be quite complementary to those of the recent mean-field studies of thermal properties of asymmetric NM using different choices of the in-medium NN interaction [33–35] as well as the RMF studies [36, 37]. The HF results obtained for the EOS of hot  $\beta$ -stable PNS matter in both the  $\nu$ -free and  $\nu$ -trapped scenarios are presented in Sec. III, where the impact of the nuclear symmetry energy and nucleon effective mass on the hydrostatic configuration of hot PNS at the total entropy per baryon  $S/A = 1, 2$  and  $4$  was found very significant. The  $\nu$ -free PNS configuration at  $S/A = 4$  was studied in details in view of the results of hydrodynamic simulation by Hempel *et al.* [9], which show that the neutrino-poor PNS matter with  $S/A \approx 4$  occurs at the onset of a  $40 M_\odot$  protonneutron progenitor collapse to black hole. The summary and main conclusions of the present research are given in Sec. V.

## II. HARTREE-FOCK CALCULATION OF HOT NUCLEAR MATTER

In our consistent HF approach, we consider a homogeneous spin-saturated NM over a wide range of the neutron and proton number densities,  $n_n$  and  $n_p$ , or equivalently of the total nucleon number density  $n_b = n_n + n_p$  (hereafter referred to as baryon density) and the

neutron-proton asymmetry  $\delta = (n_n - n_p)/(n_n + n_p)$ . Given the direct ( $v_D$ ) and exchange ( $v_{EX}$ ) parts of the (central) in-medium NN interaction  $v_c$ , the total energy density of NM at the given baryon density and temperature  $T$  is determined as

$$E(T, n_b, \delta) = E_{\text{kin}}(T, n_b, \delta) + E_{\text{pot}}(T, n_b, \delta), \quad (1)$$

where the kinetic and HF potential energy densities are determined as

$$E_{\text{kin}}(T, n_b, \delta) = \sum_{k\sigma\tau} n_{\sigma\tau}(\mathbf{k}, T) \frac{\hbar^2 k^2}{2m_\tau} \quad (2)$$

$$E_{\text{pot}}(T, n_b, \delta) = \frac{1}{2} \sum_{k\sigma\tau} \sum_{k'\sigma'\tau'} n_{\sigma\tau}(\mathbf{k}, T) n_{\sigma'\tau'}(\mathbf{k}', T) [\langle \mathbf{k}\sigma\tau, \mathbf{k}'\sigma'\tau' | v_D | \mathbf{k}\sigma\tau, \mathbf{k}'\sigma'\tau' \rangle + \langle \mathbf{k}\sigma\tau, \mathbf{k}'\sigma'\tau' | v_{EX} | \mathbf{k}'\sigma\tau, \mathbf{k}\sigma'\tau' \rangle] \quad (3)$$

$$\equiv \frac{1}{2} \sum_{k\sigma\tau} \sum_{k'\sigma'\tau'} n_{\sigma\tau}(\mathbf{k}, T) n_{\sigma'\tau'}(\mathbf{k}', T) \langle \mathbf{k}\sigma\tau, \mathbf{k}'\sigma'\tau' | v_c | \mathbf{k}\sigma\tau, \mathbf{k}'\sigma'\tau' \rangle_{\mathcal{A}}. \quad (4)$$

The single-particle wave function  $|\mathbf{k}\sigma\tau\rangle$  is plane wave, and the summation in Eqs. (2)-(4) is done separately over the neutron ( $\tau = n$ ) and proton ( $\tau = p$ ) single-particle indices. The nucleon momentum distribution  $n_{\sigma\tau}(\mathbf{k}, T)$  in the hot, spin-saturated NM is given by the Fermi-Dirac distribution

$$n_{\sigma\tau}(\mathbf{k}, T) \equiv n_\tau(n_b, \mathbf{k}, \delta, T) = \frac{1}{1 + \exp\{[\varepsilon_\tau(n_b, \mathbf{k}, \delta, T) - \mu_\tau]/T\}}. \quad (5)$$

Here  $T$  is the temperature (in MeV) and  $\mu_\tau$  is the nucleon chemical potential. The single-particle energy  $\varepsilon_\tau$  is given by

$$\varepsilon_\tau(n_b, \mathbf{k}, \delta, T) = \frac{\partial E(T)}{\partial n_\tau(n_b, \mathbf{k}, \delta, T)} = \frac{\hbar^2 k^2}{2m_\tau} + U_\tau(n_b, \mathbf{k}, \delta, T), \quad (6)$$

which is the change of the total NM energy caused by the removal or addition of a nucleon with the momentum  $k$ . At zero temperature, the nucleon momentum distribution (5) is reduced to the step function determined with the Fermi momentum  $k_F^{(\tau)} = (3\pi^2 n_\tau)^{1/3}$

$$n_\tau(n_b, k, \delta) = \begin{cases} 1 & \text{if } k \leq k_F^{(\tau)} \\ 0 & \text{otherwise.} \end{cases} \quad (7)$$

The single-particle potential  $U_\tau$  consists of the HF term and rearrangement term (RT)

$$U_\tau(n_b, \mathbf{k}, \delta, T) = U_\tau^{(\text{HF})}(n_b, \mathbf{k}, \delta, T) + U^{(\text{RT})}(n_b, \mathbf{k}, \delta, T), \quad (8)$$

$$\text{where } U_\tau^{(\text{HF})}(n_b, \mathbf{k}, \delta, T) = \sum_{k'\sigma'\tau'} n_{\tau'}(n_b, \mathbf{k}', \delta, T) \langle \mathbf{k}\sigma\tau, \mathbf{k}'\sigma'\tau' | v_c | \mathbf{k}\sigma\tau, \mathbf{k}'\sigma'\tau' \rangle_{\mathcal{A}} \quad (9)$$

$$\begin{aligned} \text{and } U_\tau^{(\text{RT})}(n_b, \mathbf{k}, \delta, T) = & \frac{1}{2} \sum_{k_1\sigma_1\tau_1} \sum_{k_2\sigma_2\tau_2} n_{\tau_1}(n_b, \mathbf{k}_1, \delta, T) n_{\tau_2}(n_b, \mathbf{k}_2, \delta, T) \\ & \times \left\langle \mathbf{k}_1\sigma_1\tau_1, \mathbf{k}_2\sigma_2\tau_2 \left| \frac{\partial v_c}{\partial n_\tau(n_b, \mathbf{k}, \delta, T)} \right| \mathbf{k}_1\sigma_1\tau_1, \mathbf{k}_2\sigma_2\tau_2 \right\rangle_{\mathcal{A}}. \end{aligned} \quad (10)$$

At zero temperature, when the nucleon momentum approaches the Fermi momentum ( $k \rightarrow k_F^{(\tau)}$ ),  $\varepsilon_\tau(n_b, k_F^{(\tau)}, \delta, T = 0)$  determined from Eqs. (6)-(10) is exactly the Fermi energy given by the Hugenholtz - van Hove theorem [38], which gives rise naturally to the RT of the single-particle potential if the in-medium NN interaction  $v_c$  is density dependent. At finite temperature  $T$ , the single-particle potential (8) is determined by an iterative procedure, with the chemical potential  $\mu_\tau$  being determined at each iteration by normalizing the nucleon momentum distribution (5) to the nucleon number density  $n_\tau$

$$n_\tau = \frac{g}{(2\pi)^3} \int n_\tau(n_b, \mathbf{k}, \delta, T) d\mathbf{k}, \quad (11)$$

where  $g = 2$  is the spin degeneracy factor. The thermodynamic equilibrium of hot NM is directly associated with the evolution of the entropy. Given the NM energy density obtained microscopically (in terms of the nucleon degrees of freedom) in the HF calculation (1)-(4) using the realistic effective NN interaction between nucleons in medium, it is natural to determine the baryon entropy density  $S$  of asymmetric NM on the same level, using the functional form for the entropy density of a Fermi-Dirac gas at the given temperature  $T$  and baryon density  $n_b$

$$\begin{aligned} S(T, n_b, \delta) = & \frac{g}{8\pi^3} \sum_{\tau} \int \{ n_\tau(n_b, \mathbf{k}, \delta, T) \ln[n_\tau(n_b, \mathbf{k}, \delta, T)] \\ & + [1 - n_\tau(n_b, \mathbf{k}, \delta, T)] \ln[1 - n_\tau(n_b, \mathbf{k}, \delta, T)] \} d\mathbf{k}. \end{aligned} \quad (12)$$

Thus, the entropy density (12) is affected by different nuclear EOS's via the corresponding nucleon mean-field potentials entering the nucleon momentum distribution (5).

The Helmholtz free energy density is determined as  $F(T) = E(T) - TS(T)$ . Dividing (1) and (12) over the total baryon number density  $n_b$ , we obtain the internal energy per particle  $E(T)/A$  and the entropy per particle  $S(T)/A$  that are used to determine the (density

TABLE I: HF results for the NM saturation properties obtained at  $n_b = n_0$  and  $T = 0$ , using the considered effective NN interactions. The nucleon effective mass  $m^*/m$  is evaluated at  $\delta = 0$  and  $E_0 = E(T = 0, n_0, \delta = 0)/A$ .  $K_{\text{sym}}$  is the curvature parameter of the symmetry energy (20), and  $K_\tau$  is the symmetry term of the nuclear incompressibility (21) determined at the saturation density  $n_\delta$  of asymmetric NM.

Model	$n_0$ (fm <sup>-3</sup> )	$E_0$ (MeV)	$K_0$ (MeV)	$m^*/m$	$J$ (MeV)	$L$ (MeV)	$K_{\text{sym}}$ (MeV)	$K_\tau$ (MeV)	Ref.
CDM3Y3	0.17	-15.9	218	0.706	30.1	49.6	-23	-181	[39]
CDM3Y6	0.17	-15.9	252	0.706	30.1	49.7	-29	-245	[39]
CDM3Y3s	0.17	-15.9	218	0.706	32.0	49.1	-140	-297	[8]
CDM3Y6s	0.17	-15.9	252	0.706	32.0	49.1	-154	-370	[8]
M3Y-P5	0.16	-16.1	235	0.637	30.9	27.9	-229	-339	[27]
M3Y-P7	0.16	-16.0	254	0.589	33.0	54.3	-138	-395	[28]
D1N	0.16	-16.0	221	0.748	30.1	32.4	-182	-319	[30]
SLy4	0.16	-16.0	230	0.694	32.1	46.0	-120	-332	[32]

dependent) free energy per particle and the pressure of hot asymmetric NM as

$$\frac{F(T, n_b, \delta)}{A} = \frac{E(T, n_b, \delta)}{A} - T \frac{S(T, n_b, \delta)}{A}, \quad P(T, n_b, \delta) = n_b^2 \frac{\partial [F(T, n_b, \delta)/A]}{\partial n_b}. \quad (13)$$

Thus, the EOS at finite temperature is given by Eq. (13). The different EOS's of symmetric NM are usually distinguished by the value of nuclear incompressibility  $K_0$ , determined at the nucleon saturation density ( $n_0 \approx 0.17 \text{ fm}^{-3}$ ) and zero temperature as

$$K_0 = 9n_b^2 \frac{\partial^2}{\partial n_b^2} \left[ \frac{E(T=0, n_b, \delta=0)}{A} \right]_{n_b=n_0}. \quad (14)$$

Like in Ref. [8], we have used in the present HF calculation two different sets of the density-dependent M3Y interaction. The first set, dubbed as CDM3Yn (n=3,6), is the original M3Y-Paris interaction [21] supplemented by an *isoscalar* (IS) density dependence that was parametrized [23] to reproduce the saturation properties of cold symmetric NM and give the different nuclear incompressibilities  $K_0$  shown in Table I. These interactions, especially the CDM3Y6 version, have been widely tested in numerous folding model analyses of the nucleus-nucleus elastic scattering [25] and charge-exchange scattering to the isobar analog states [24, 47]. The *isovector* (IV) density dependence of the CDM3Yn interaction was first parametrized to reproduce the BHF results for the density- and isospin dependent nucleon optical potential of Jeukenne, Lejeune and Mahaux (JLM) [48, 49]. Then, the

total IV strength of the CDM3Yn interaction was fine-tuned to reproduce the measured charge-exchange ( $p, n$ ) and ( $^3\text{He}, t$ ) data for the isobar analog states [24, 47]. In our recent extended HF study of the single-particle potential in the NM [39], the parameters of the IV density dependence of the CDM3Yn interactions have been redetermined with a consistent inclusion of the rearrangement term into the single-nucleon potential at different NM densities. At variance with the CDM3Yn interactions, the M3Y-Pn interactions (n=5 and 7) have been carefully parametrized by Nakada [26–28] in terms of the finite-range M3Y interaction supplemented with a zero-range density-dependent term, to consistently reproduce the NM saturation properties and ground-state (g.s.) structure of the stable nuclei as well as the dripline nuclei. In particular, the newly parametrized M3Y-P7 version [28] gives a stable description of symmetric NM up to the baryon density as high as  $6n_0$ , while retaining a realistic description of the g.s. structure of finite nuclei. For comparison, the present HF calculation has also been done using the two other popular choices of the effective NN interaction: the D1N version of Gogny interaction [30] and SLy4 version [31] of Skyrme interaction [32]. The explicit parametrizations of the density dependent NN interactions used in the present HF calculation are presented and discussed in more details in Appendices A and B. The NM saturation properties at zero temperature given by different density dependent interactions are presented in Table I. One can see that all interactions under study give reasonable description of the bulk properties of NM at the saturation density  $n_0$ , excepting the nucleon effective mass given by the M3Y-Pn interactions that is significantly lower than the empirical value around 0.72 [50]. Given the HF mean field potentials based on various density dependent NN interactions (see Table I), it is important to make some comparison of the present HF results with those of a microscopic many-body calculation starting from the realistic free NN interaction. In the present work we have focused on the microscopic EOS of hot asymmetric NM from the BHF calculation by Burgio and Schulze [12], using the Argonne NN interaction (V18 version [51] with the Urbana three-body force). This microscopic EOS has been used to study the composition of hot  $\beta$ -stable PNS matter and estimate the maximum gravitational mass of PNS at entropy  $S/A=1$  and 2. One can see in Fig. 1 that the HF results obtained with the CDM3Y6 and CDM3Y3 interactions for the free energy per particle  $F/A$  at different temperatures are in good agreement with the microscopic BHF results (reproduced here from the analytical expressions fitted by the authors of Ref. [12]). A slight difference between the results given by the CDM3Y6 and

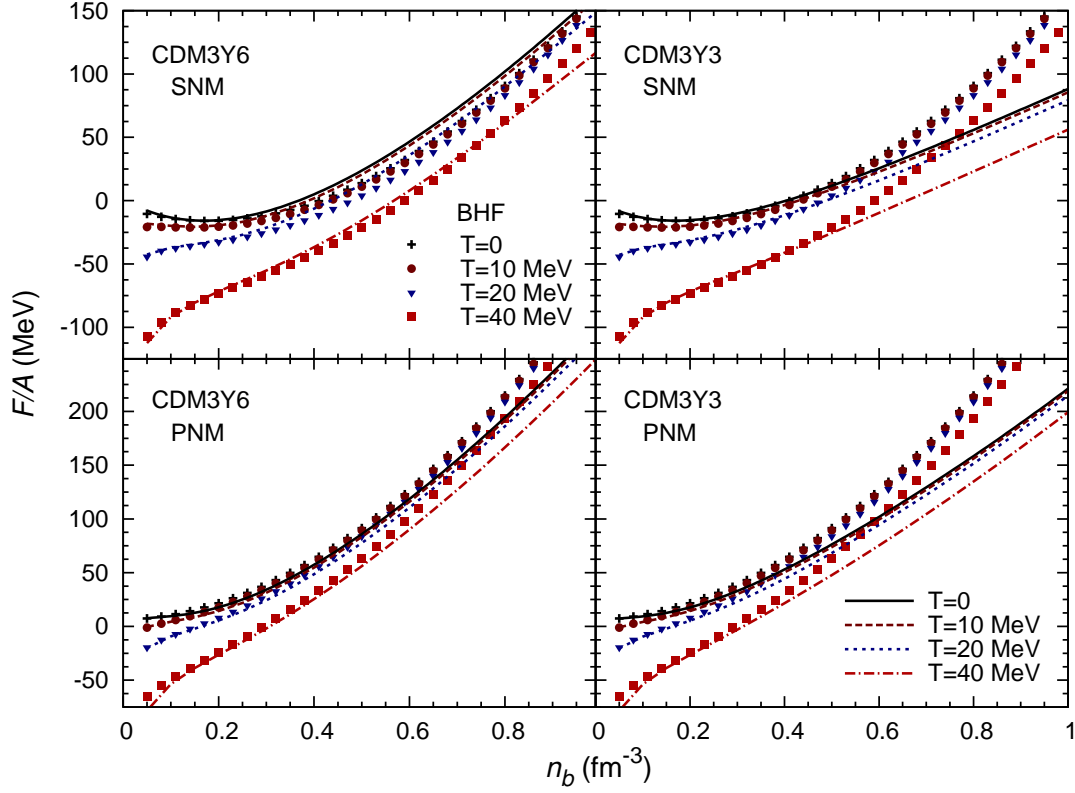


FIG. 1: (Color online) Free energy per particle  $F/A$  of symmetric nuclear matter (SNM) and pure neutron matter (PNM) at different temperatures given by the HF calculation (1)-(13) using the CDM3Y3 (right panel) and CDM3Y6 (left panel) interactions [39] (lines), in comparison with the BHF results (symbols) by Burgio and Schulze [12].

CDM3Y3 interactions at high NM densities is mainly due to the different incompressibilities  $K_0$  given by these two interactions. Over the whole range of NM densities up to  $n_b = 1 \text{ fm}^{-3}$ , the  $F/A$  values given by the CDM3Y6 interaction are very close to the BHF results [12]. The  $F/A$  values given by the M3Y-P5 and M3Y-P7 interactions are compared with the BHF results in Fig. 2, and a better agreement with the BHF results for pure neutron matter is achieved with the newly parametrized and improved M3Y-P7 version [28]. A similar comparison of the free energy given by the D1N version [30] of Gogny interaction and SLy4 version [32] of Skyrme interaction with the BHF results is shown in Fig. 3. We found that the results given by the D1N interaction for pure neutron matter differ strongly from the BHF results at high NM densities, while those given by the Sly4 interaction agree reasonably with the BHF results for both the symmetric NM and pure neutron matter over a wide range of NM densities. Note that the free energy given by Sly4 interaction at high



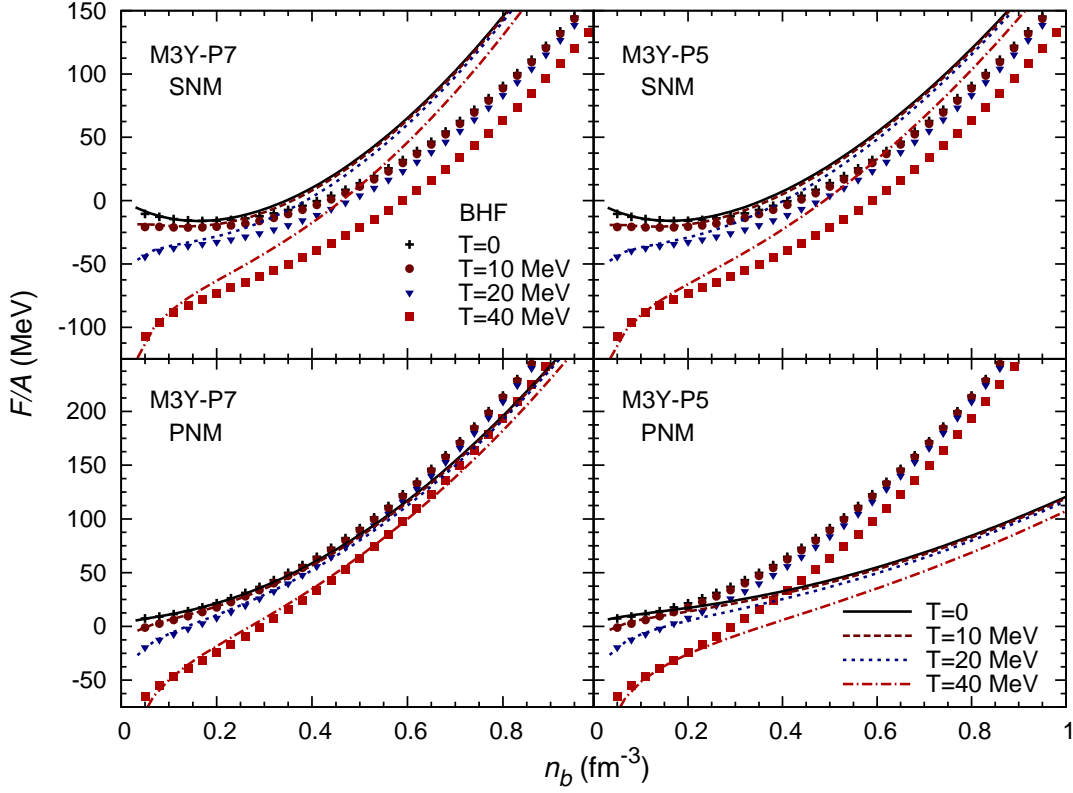


FIG. 2: (Color online) The same as Fig. 1 but for the HF results obtained with the M3Y-P5 (right panel) and M3Y-P7 (left panel) interactions parametrized by Nakada [27, 28].

baryon densities depends weakly on temperature because the internal NM energy obtained with the zero-range Skyrme interaction [see Appendix B] is *temperature independent*.

### A. The nuclear symmetry energy at finite temperature

The difference between the free energy per particle of asymmetric NM and that of symmetric NM determines the *free symmetry energy* per particle

$$\frac{F_{\text{sym}}(T, n_b, \delta)}{A} = \frac{F(T, n_b, \delta)}{A} - \frac{F(T, n_b, \delta = 0)}{A}. \quad (15)$$

It is often assumed [12, 13], like at the zero temperature, that the free symmetry energy per particle also depends *quadratically* on the neutron-proton asymmetry  $\delta$  as

$$\frac{F_{\text{sym}}(T, n_b, \delta)}{A} \approx f_{\text{sym}}(T, n_b) \delta^2 + O(\delta^4), \quad (16)$$

and one needs only to determine the free energy of symmetric NM and that of pure neutron matter for the study of hot asymmetric NM. The free energy of asymmetric NM at any

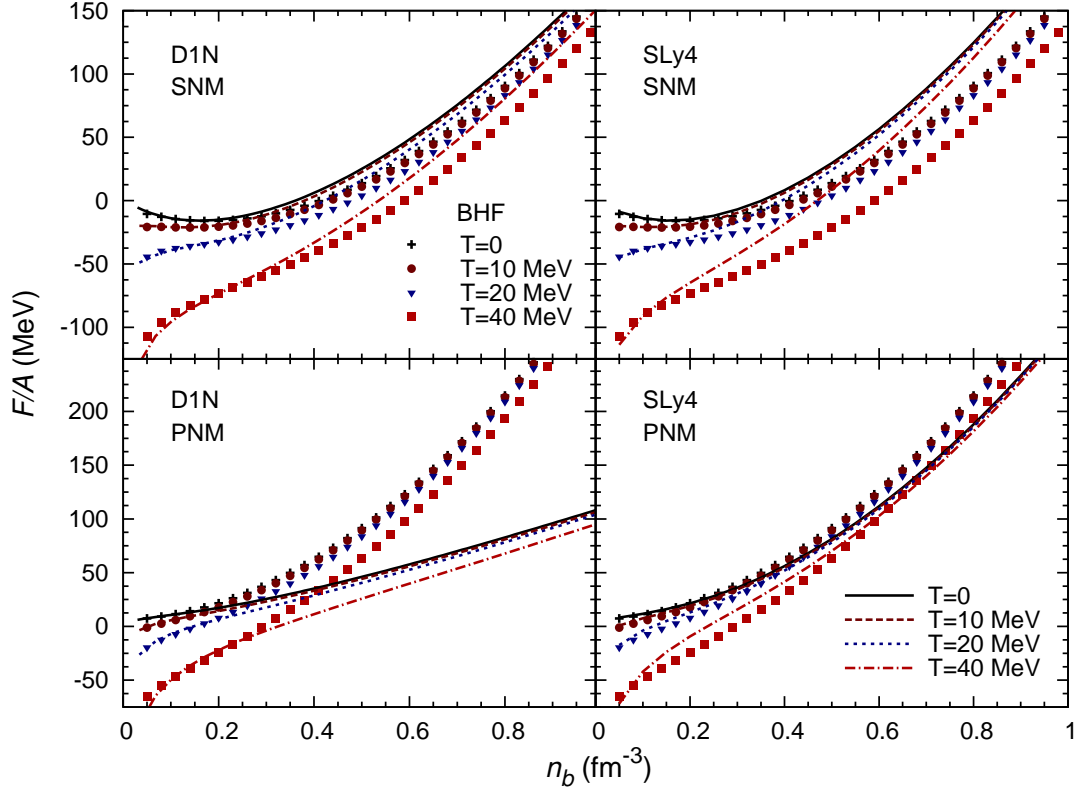


FIG. 3: (Color online) The same as Fig. 1 but for the HF results obtained with the D1N version [30] of Gogny interaction (left panel) and SLy4 version [32] of Skyrme interaction (right panel).

neutron-proton asymmetry  $\delta$  can then be estimated using Eq. (16). However, as shown below, the quadratic approximation (16) becomes much poorer with the increasing  $\delta$  and  $T$ . In fact, the quadratic approximation is reasonable only for the internal symmetry energy

$$\frac{E_{\text{sym}}(T, n_b, \delta)}{A} = \frac{E(T, n_b, \delta)}{A} - \frac{E(T, n_b, \delta = 0)}{A} \approx \varepsilon_{\text{sym}}(T, n_b) \delta^2 + O(\delta^4). \quad (17)$$

In the thermodynamic equilibrium, it is illustrative to express the free symmetry energy per particle as

$$\frac{F_{\text{sym}}(T, n_b, \delta)}{A} = \frac{E_{\text{sym}}(T, n_b, \delta)}{A} - T \frac{S_{\text{sym}}(T, n_b, \delta)}{A}, \quad (18)$$

where  $S_{\text{sym}}(T, n_b, \delta)/A$  is the symmetry part of the entropy per particle

$$\frac{S_{\text{sym}}(T, n_b, \delta)}{A} = \frac{S(T, n_b, \delta)}{A} - \frac{S(T, n_b, \delta = 0)}{A} \quad (19)$$

A comparison of the HF results for the free symmetry energy with those given by the microscopic BHF calculation (reproduced from the fitted analytical expression given in Ref. [12]) is much more drastic, because  $F_{\text{sym}}/A$  is directly determined by the isospin dependence of

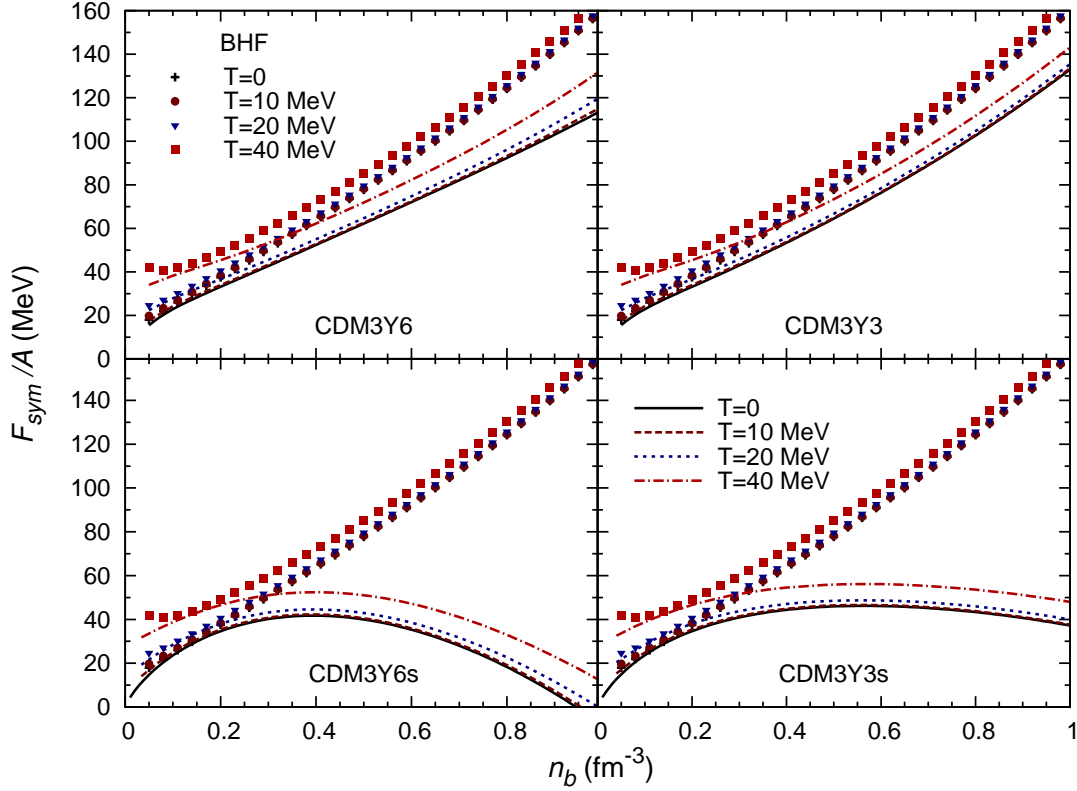


FIG. 4: (Color online) Free symmetry energy per particle  $F_{\text{sym}}/A$  of pure neutron matter ( $\delta = 1$ ) at different temperatures given by the HF calculations (15) using the CDM3Y3 and CDM3Y6 interactions [39] and their soft versions CDM3Y3s and CDM3Y6s [8] (lines), in comparison with the BHF results (symbols) by Burgio and Schulze [12].

the considered NN interactions. As can be seen in Fig. 4, the free symmetry energy predicted by the HF calculation using the CDM3Y6 and CDM3Y3 interactions agree well with the BHF results. Because the isovector density dependence of these two interactions has been fine tuned [24, 39] to reproduce the density dependence of the nucleon optical potential obtained in the BHF calculation by the JLM group [48], both the CDM3Y3 and CDM3Y6 interactions give a *stiff* density dependence of the free symmetry energy at different temperatures. To illustrate this we also used the *soft* versions (CDM3Y3s and CDM3Y6s) of these interactions, where the IV density dependence  $F_1(n_b)$  was assumed to be the same as the IS density dependence  $F_0(n_b)$  [8]. One can see that the soft free symmetry energy fails to agree with the BHF results soon after the baryon density exceeds the saturation density  $n_0$  (see lower panel of Fig. 4). The free symmetry energy given by the M3Y-Pn, D1N, and SLy4 interactions also disagree strongly with the BHF results (see Fig. 5) at high NM densi-

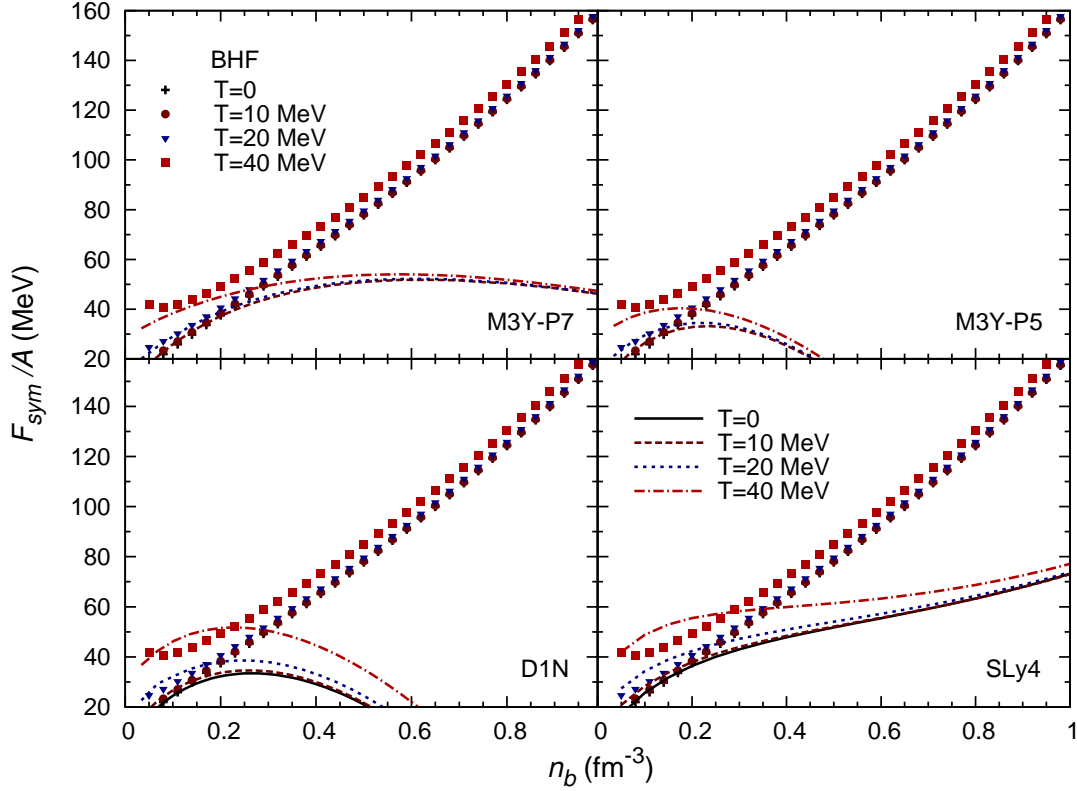


FIG. 5: (Color online) The same as Fig. 4 but for the HF results given by the M3Y-P5 and M3Y-P7 interactions parametrized by Nakada [27, 28], and the D1N version [30] of Gogny interaction and SLy4 version [32] of Skyrme interaction.

ties, although the isospin dependence of these interactions was carefully tailored to give the good description of the g.s. structure of the neutron-rich dripline nuclei [27, 28, 30]. These two different behaviors have been observed earlier [19] and are discussed in the literature as the *asy-stiff* (with the symmetry energy steadily increasing with the NM density) and *asy-soft* (with the symmetry energy reaching its saturation and then decreasing to negative values at high NM densities) behaviors. In this context, the CDM3Y3, CDM3Y6, and Sly4 interactions are *asy-stiff*, while the CDM3Y3s, CDM3Y6s, M3Y-P5, M3Y-P7, and D1N interactions are *asy-soft*. It can be seen in Figs. 4 and 5 that the finite-temperature effect does not change this classification. It should be noted that, like the BHF calculation, the most recent nonrelativistic mean-field studies of hot asymmetric NM [33, 34] as well as the RMF studies [36, 37] also predict the *asy-stiff* behavior of the free symmetry energy.

We have further checked the dependence of the free symmetry energy on the neutron-proton asymmetry  $\delta$  by performing finite-temperature HF calculations at different  $\delta$  values,

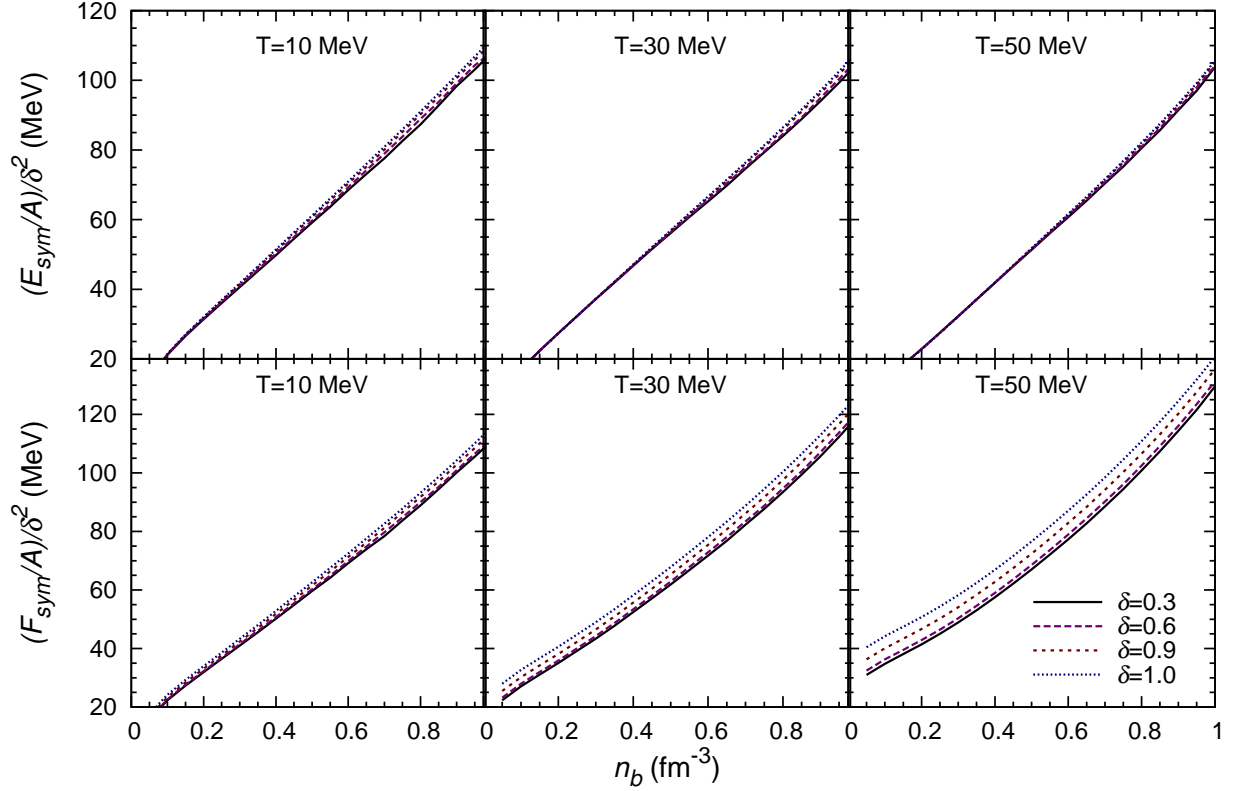


FIG. 6: (Color online) Free symmetry energy (15) (lower panel) and internal symmetry energy (17) (upper panel) at different temperatures, given by the HF calculation using the CDM3Y6 interaction [39].  $(F_{\text{sym}}/A)/\delta^2$  curves must be very close if the quadratic approximation (16) is valid.

and it turned out that the quadratic approximation (16) becomes much poorer with the increasing temperature as shown in lower panel of Fig. 6, where all  $(F_{\text{sym}}/A)/\delta^2$  curves should be very close if the quadratic approximation (16) is valid. Such a breakdown of the quadratic approximation, sometimes also dubbed as the parabolic law, is clearly due to the effect of finite entropy. Therefore, the free symmetry energy of hot asymmetric NM needs to be calculated explicitly at different neutron-proton asymmetries  $\delta$  without using the approximation (16). To further illustrate this effect, we have plotted the HF results for the internal symmetry energy per particle  $E_{\text{sym}}/A$  in the upper panel of Fig. 6, and one can see that the quadratic approximation (17) remains reasonable for  $E_{\text{sym}}/A$  at different temperatures.

At zero temperature,  $\varepsilon_{\text{sym}}$  determined at the saturation density  $n_b = n_0$  is known as the symmetry energy coefficient  $J$  which has been predicted by numerous many-body calculations to be around 30 MeV. The symmetry energy of cold NM can be expanded around  $n_0$

[40, 41] as

$$\varepsilon_{\text{sym}}(T=0, n_b) = J + \frac{L}{3} \left( \frac{n_b - n_0}{n_0} \right) + \frac{K_{\text{sym}}}{18} \left( \frac{n_b - n_0}{n_0} \right)^2 + \dots \quad (20)$$

where  $L$  and  $K_{\text{sym}}$  are the slope and curvature parameters of the symmetry energy. The asymmetric NM with the neutron-proton asymmetry  $\delta \lesssim 0.75$  can still be saturated by the nuclear mean field, but at the baryon number density significantly lower than that of symmetric NM ( $n_\delta < n_0$ ) [22]. As shown by Piekarewicz and Centelles [41], the nuclear incompressibility at the new saturation density  $n_\delta$  can be approximated by a quadratic dependence on the neutron-proton asymmetry  $\delta$

$$K(n_\delta) \approx K_0 + K_\tau \delta^2 + O(\delta^4). \quad (21)$$

We have calculated the symmetry term  $K_\tau$  of the nuclear incompressibility  $K(n_\delta)$  based on Eq. (18c) in Ref. [41], using different density dependent NN interactions under the present study. The obtained  $K_\tau$  values of -180 to -395 MeV (see Table I) turned out to be smaller (in  $|K_\tau|$  value) than  $K_\tau^{(\text{exp})} \approx -550 \pm 100$  MeV deduced from the measured strength distribution of giant monopole resonance (GMR) in neutron-rich tin isotopes [42]. Such a disagreement was found also with different versions of Skyrme interaction [42] and FSUGold interaction that was well tested in the RMF studies of GMR in heavy nuclei [41]. This remains an open question that might be linked to large uncertainties in extrapolating  $K_\tau$  values for asymmetric NM from the GMR data measured for finite nuclei [41].

The knowledge about the density dependence of the nuclear symmetry energy is vital for the construction of the EOS of asymmetric NM. The widely used method to probe the NM symmetry energy associated (in the mean-field scheme) with a given in-medium NN interaction is to test such an interaction in the nuclear reaction and/or the nuclear structure studies involving nuclei with the large neutron excess. Based on the physics constraints implied by such studies, the extrapolation is made to draw the conclusion on the low- and high-density behavior of the symmetry energy (see a recent review [43] for more details). For example, the parameters  $J$ ,  $L$ , and  $K_{\text{sym}}$  of the expansion (20) have been the subject of several nuclear structure studies, where one tries to deduce constraints for these 3 parameters from the observation of the monopole, dipole, and spin-dipole resonances [44]. Note that higher-order term  $O(\delta^4)$  in the expansion (17) of the symmetry energy at zero temperature might be needed for a more precise determination of the slope parameter  $L$  [45]. Quite a robust constraint for both the  $J$  and  $L$  values has been established [46] based on several tens

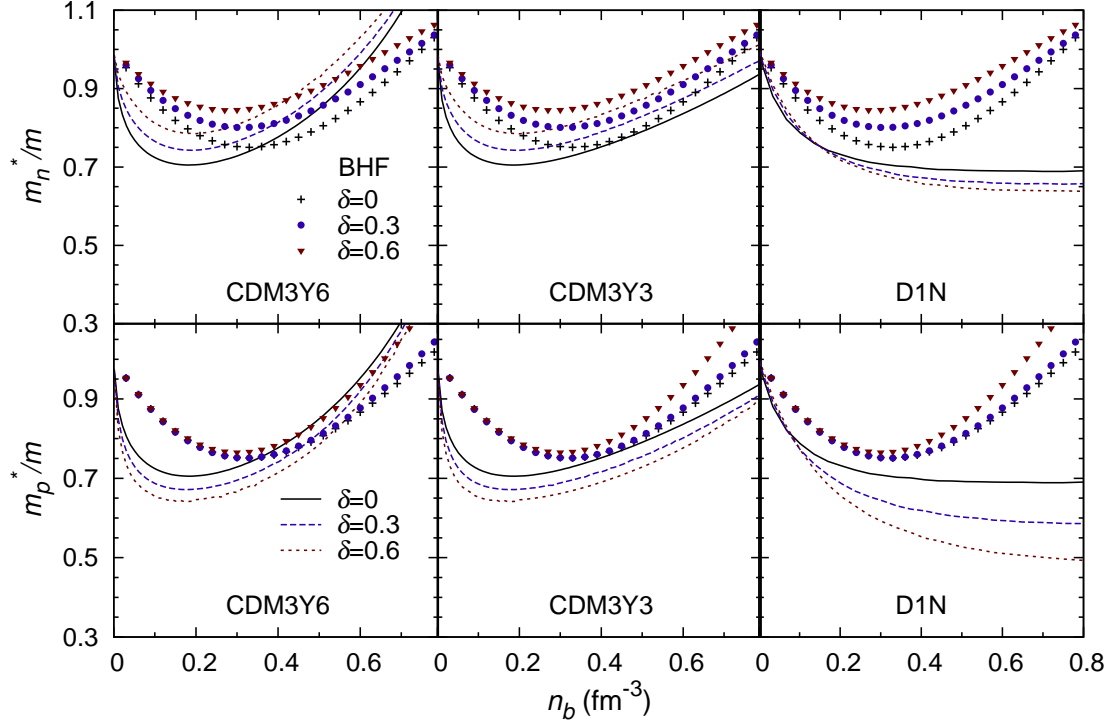


FIG. 7: (Color online) Density profile of the neutron- (upper panel) and proton effective mass (lower panel) at different neutron-proton asymmetries  $\delta$  given by the HF calculation using the CDM3Y6 and CDM3Y3 interactions [39], and the D1N version of Gogny interaction [30], in comparison with the BHF results (symbols) by Baldo *et al.* [52].

analyses of the terrestrial nuclear physics experiments and astrophysical observations, which give  $J \approx 31.6 \pm 2.7$  MeV and  $L \approx 58.9 \pm 16.0$  MeV. Using the parameters of the isovector density dependence of the CDM3Yn interactions determined recently in Ref. [39], the values  $J \approx 30.1$  MeV and  $L \approx 49.7$  MeV given by the HF calculation of cold asymmetric NM are well within this empirical range. In our previous HF study [8] of cold ( $\beta$ -stable) neutron star matter, the baryon and lepton compositions in the core of neutron star as well as its maximum gravitational mass and radius were shown to be strongly affected by the slope of the nuclear symmetry energy at high baryon densities. The extension of the mean-field approach of Ref. [8] to study the impact of the symmetry energy to the composition of hot  $\beta$ -stable PNS matter is presented in the next Section.

## B. The nucleon effective mass and thermal properties of NM

A very important physics quantity associated with the momentum dependence of the single-nucleon potential (8) is the (density dependent) nucleon effective mass, determined within the nonrelativistic mean-field formalism as

$$\frac{m_\tau^*(n_b, \delta)}{m} = \left[ 1 + \frac{m}{\hbar^2 k_F^{(\tau)}} \frac{\partial U_\tau(n_b, \delta, k)}{\partial k} \bigg|_{k_F^{(\tau)}} \right]^{-1}, \quad (22)$$

where  $m$  is the free nucleon mass. Given the finite range of the Yukawa (or Gaussian) function used to construct the radial part of the CDM3Yn, M3Y-Pn, and Gogny interactions, the single-particle potential depends explicitly on the nucleon momentum  $k$  via its exchange term [see Eqs. (A20) and (A25) in Appendix A] that implies a *nonlocal* single-particle potential in the coordinate space. Therefore, the nucleon effective mass  $m^*$  is a measure of nonlocality of the mean-field potential felt by a nucleon propagating in nuclear medium. Because of the zero range of Skyrme interaction, the corresponding mean-field potential is always local, and the momentum dependence of Skyrme interaction has to be included explicitly [see Eq. (B1) in Appendix B]. In general, the nucleon effective mass is linked closely to several important nuclear physics phenomena, like the dynamics of HI collisions, damping of giant resonances, temperature profile and cooling of hot PNS and neutrino emission therefrom [11, 52, 53]. Moreover, the density dependence of nucleon effective mass was shown to be directly related to the thermodynamic properties of NM [11, 54]. For example, in the degenerate limit of symmetric NM or pure neutron matter with  $T \ll T_F$ , the entropy per particle and temperature at the given Fermi momentum  $k_F$  can be approximately expressed [11] as

$$\frac{S}{A} \approx \frac{\pi^2}{2} \frac{T}{T_F}, \text{ where the Fermi temperature } T_F = \frac{\hbar^2 k_F^2}{2m^*}. \quad (23)$$

For a comparison with the BHF results for the nucleon effective mass at different NM densities [52], we have evaluated the neutron- and proton effective mass (22) from the HF single-particle potential at zero temperature. The density dependence of the neutron- and proton effective mass at different neutron-proton asymmetries  $\delta$  given by different density dependent NN interactions are compared with the BHF results in Figs. 7 and 8. To be consistent with the discussion on results shown in Figs. 1-5, we have plotted in Figs. 7 and 8



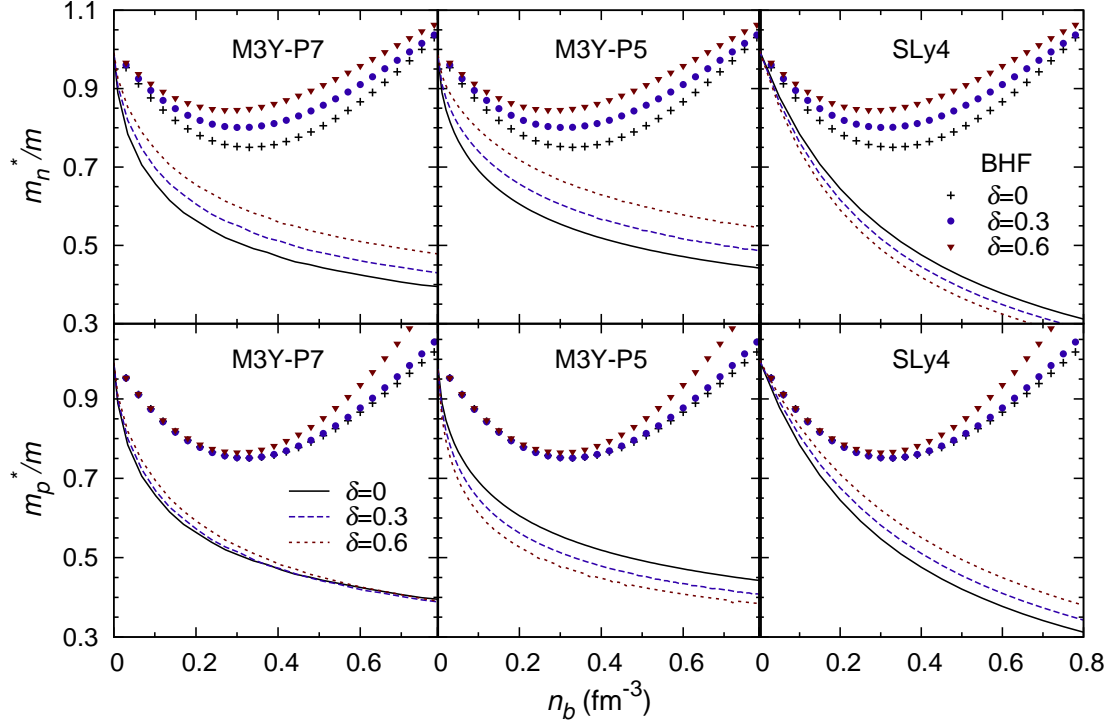


FIG. 8: (Color online) The same as Fig. 7 but for the HF results obtained with the M3Y-P7 and M3Y-P5 interactions [27, 28], and the SLy4 version [32] of Skyrme interaction.

the results of the BHF calculation by Baldo *et al.* [52] (reproduced here from the analytical formulas fitted by the authors of Ref. [52]) which were also obtained with the V18 version of Argonne NN interaction [51] supplemented by the phenomenological Urbana three-body force. We found that only the CDM3Yn interactions give the neutron- and proton effective mass behaving similarly to that predicted by the BHF calculation. Namely, the  $m_\tau^*/m$  value decreases to some minimum at the baryon density  $n_b \approx 0.2 \text{ fm}^{-3}$  and then rises up to above unity at high baryon densities. Such a *saturation* trend of the nucleon effective mass was shown in the BHF calculation to be entirely due to the repulsive contribution by the three-body force (see Fig. 1 of Ref. [52]). The rise at high densities of the  $m_\tau^*/m$  value given by the CDM3Y6 interaction is stiffer than that given by the CDM3Y3 interaction, and this effect (observed at both  $\delta = 0$  and  $\delta \neq 0$ ) is mainly due to different nuclear incompressibilities  $K_0$  of cold symmetric NM determined with different IS density dependence  $F_0(n_b)$  of these interactions [see Eq. (A4) in Appendix A]. The D1N version of Gogny interaction gives a rather slowly decreasing  $m_\tau^*/m$  value with the increasing baryon density (see right panel of Fig. 7), and such a behavior of the nucleon effective mass is similar to that obtained in the

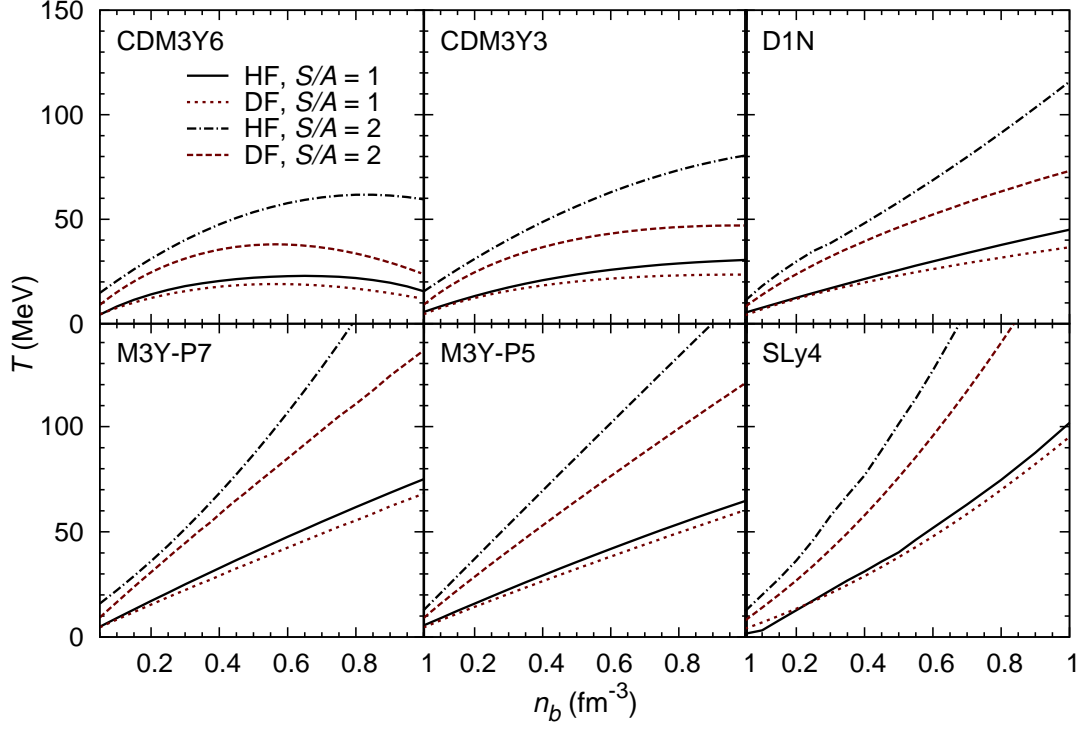


FIG. 9: (Color online) Density profile of temperature in the isentropic and symmetric NM given by the HF calculation using different density dependent NN interactions, in comparison with that given by the approximation (23) for the fully degenerate Fermi (DF) system at  $T \ll T_F$ .

recent mean-field studies using other choices of the finite-range effective NN interaction [35]. The nucleon effective mass predicted by the M3Y-Pn and Sly4 interactions (see Fig 8) fall rapidly from  $m_\tau^*/m \approx 0.6$  at  $n_b \approx 0.2 \text{ fm}^{-3}$  to low values around 0.3 at  $n_b \approx 0.8 \text{ fm}^{-3}$ . Such a behavior seems not realistic and totally opposite to that predicted by the microscopic BHF calculation [52].

The difference in nucleon effective masses given by different density dependent NN interactions shown in Figs. 7 and 8 is very significant at high baryon densities, and it must show up, therefore, also in the HF results for thermal properties of NM [11, 54]. As an illustration, the density profile of temperature of the isentropic and symmetric NM at  $S/A = 1$  and 2 deduced from the HF results given by different density dependent NN interactions is compared with that given by the full degeneracy limit (23) in Fig. 9. One can see that at low temperatures (or  $S/A = 1$ ) the HF results are rather close to those given by Eq. (23). At  $S/A = 2$  the temperature predicted by the HF calculation is larger than that given by the degeneracy limit over the whole density range, and the approximation (23) becomes worse

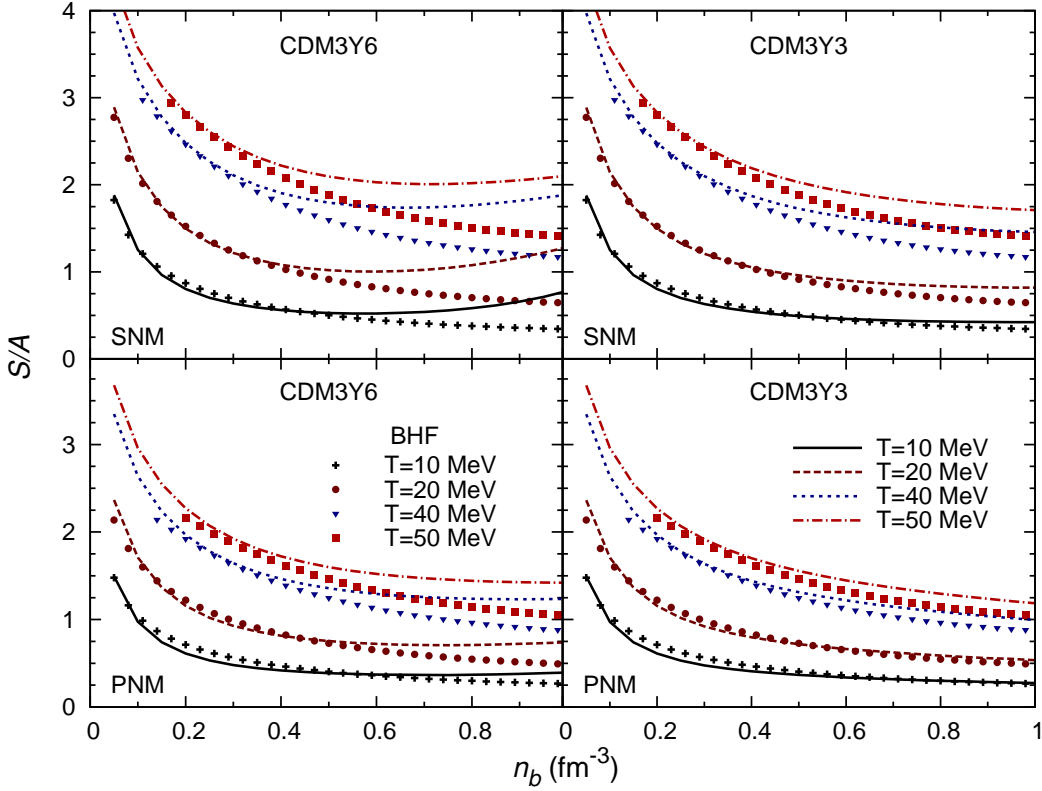


FIG. 10: (Color online) Density profile of entropy per particle  $S/A$  of symmetric nuclear matter (SNM) and pure neutron matter (PNM) at different temperatures, deduced from the HF results (lines) obtained with the CDM3Y6 and CDM3Y3 interactions [39], in comparison with the BHF results by Burgio and Schulze (symbols) [12].

at high baryon densities. Nevertheless, the trend of temperature  $T$  being proportional to the Fermi temperature  $T_F$  (or inversely proportional to nucleon effective mass) seems to hold, and at the given baryon density the lower the nucleon effective mass  $m^*$  the higher the NM temperature  $T$ . Given very low nucleon effective masses at high baryon densities predicted by the M3Y-Pn and Sly4 interactions compared to those predicted by the CDM3Yn and D1N interactions (see Fig 8), the NM temperatures predicted by the M3Y-Pn and Sly4 interactions are also substantially higher than those predicted by the CDM3Yn and D1N interactions at high baryon densities (see Fig 9). This result shows clearly a strong impact of the nucleon effective mass to the thermodynamic properties of NM.

The behavior of entropy is also an important thermodynamic property associated with the given EOS of hot NM (through the single-particle potential embedded in the nucleon

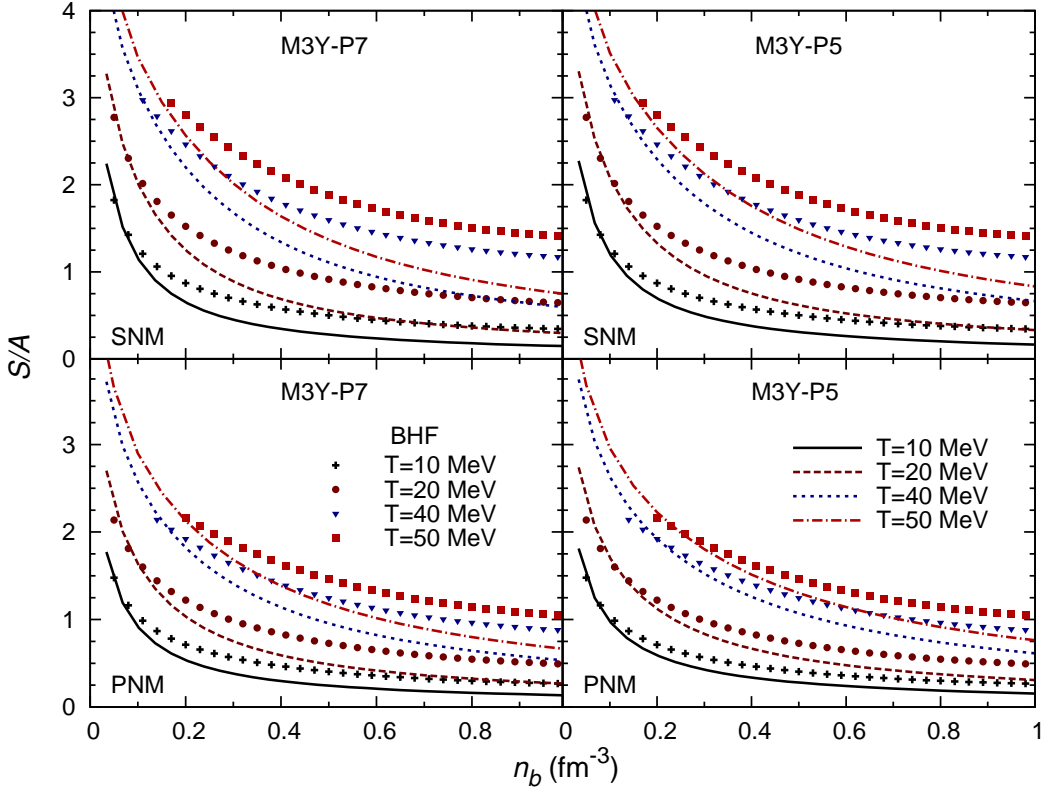


FIG. 11: (Color online) The same as Fig. 10 but for the HF results obtained with the M3Y-P7 and M3Y-P5 interactions [27, 28].

momentum distribution used to estimate  $S/A$ ). Although a constant  $S/A = 1 \sim 2$  was often assumed for the hydrostatic configuration of PNS [11], a recent hydrodynamic simulation of black hole formation in a failed core-collapse supernova [9] has shown that entropy per baryon  $S/A \approx 4$  is reached at the onset of collapse of the massive ( $40 M_\odot$ ) PNS to black hole. Therefore, the present HF calculation of hot NM has been extended to high temperatures  $T$  that correspond to  $S/A = 4$ . At  $T \leq 50$  MeV, the density profiles of entropy given by the present HF calculation are compared in Figs. 10-12 with those given by the BHF calculation [12] of symmetric NM and pure neutron matter (reproduced here from the fitted analytical expressions of the free energy in the temperature range  $0 \leq T \leq 50$  MeV [12]).

One can see in Fig. 10 that  $S/A$  values obtained with both the CDM3Y3 and CDM3Y6 interactions agree reasonably well with those given by the BHF calculation at different NM densities. At high densities up to  $n_b = 1 \text{ fm}^{-3}$ , the  $S/A$  values given by the CDM3Y3 interaction agree better with those given by the BHF calculation [12] (see right panel of

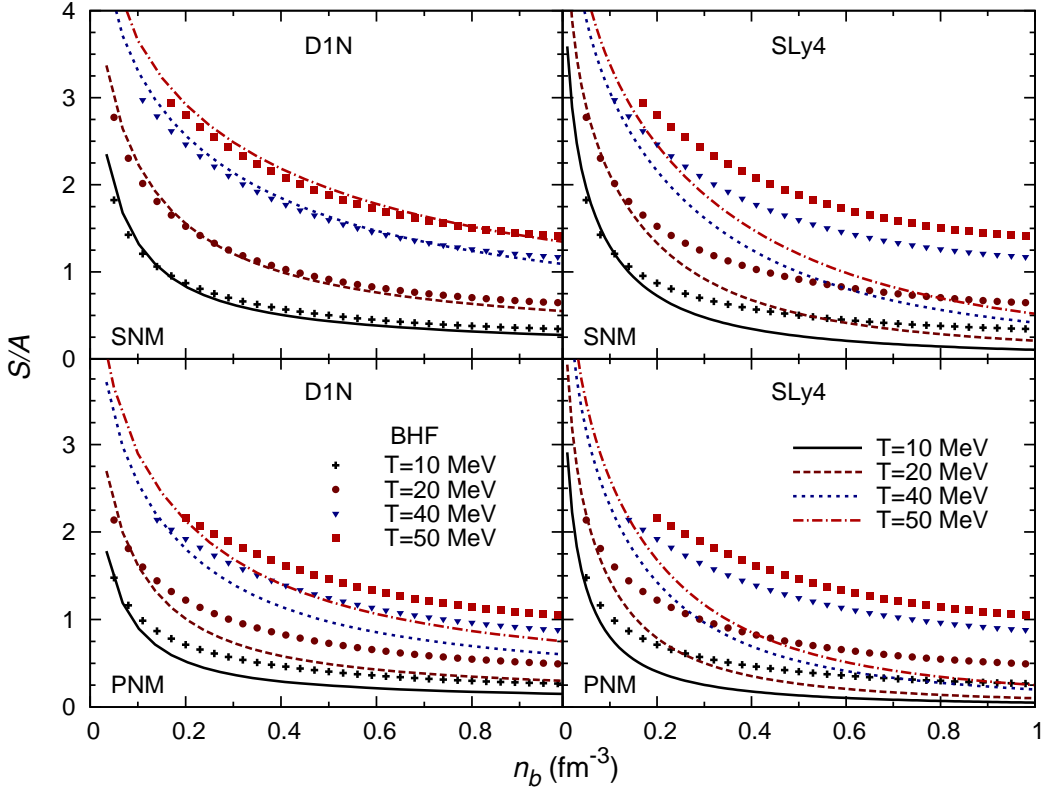


FIG. 12: (Color online) The same as Fig. 10 but for the HF results obtained with the D1N version [30] of Gogny interaction and SLy4 version [32] of Skyrme interaction.

Fig. 10). Such a difference in the calculated  $S/A$  values is directly resulted from the difference in the free energy per particle  $F/A$  (see Fig. 1), because entropy at the given baryon density can also be determined from the derivative of the free energy with respect to the temperature, instead of using Eq. (12). Therefore, the different behaviors of  $S/A$  values obtained with the two CDM3Yn interactions (found at both  $\delta = 0$  and  $\delta = 1$ ) are due mainly to different nuclear incompressibilities  $K_0$  given by these two interactions, like discussed above for the behavior of nucleon effective mass. Recall that the CDM3Y3 and CDM3Y6 interactions give  $K_0 \approx 217$  and  $252$  MeV, respectively, compared with  $K_0 \approx 210$  MeV given by the BHF calculation [12]. The density profile of  $S/A$  values given by the other interactions are plotted in Figs. 11 and 12, and the agreement with the BHF results becomes worse, especially for the Sly4 version of Skyrme interaction. The difference between  $S/A$  values given by the HF calculation using Sly4 interaction and those given by the BHF calculation is likely due to the drastic difference in the nucleon effective masses at high baryon densities (see right panel of

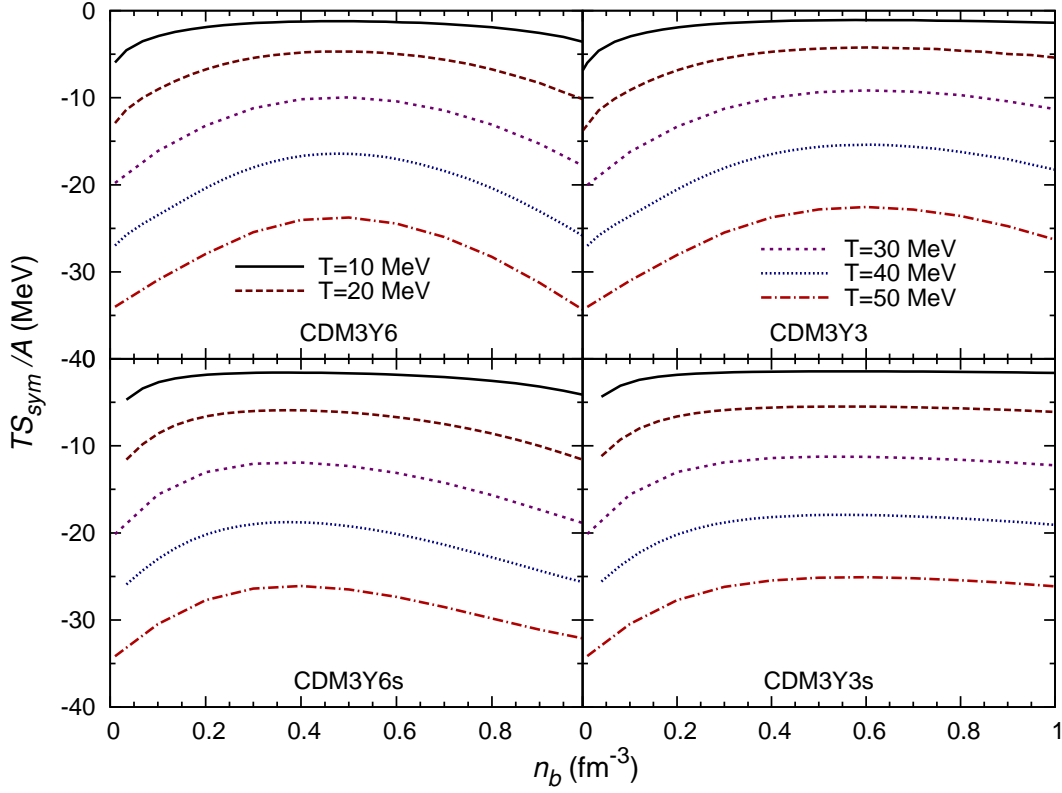


FIG. 13: (Color online) Symmetry part of the entropy per particle (19) of pure neutron matter at different temperatures given by the CDM3Y3 and CDM3Y6 interactions [39] and their soft CDM3Y3s and CDM3Y6s versions [8].  $S_{\text{sym}}/A$  is scaled by the corresponding temperature to have the curves well distinguishable at different  $T$ .

Fig. 8) which implies different momentum dependences of the single-particle potential (the key input for the HF calculation of thermal properties of NM). To explore how strong is the effect caused by different behaviors of the nuclear symmetry energy, we have plotted in Fig. 13 the symmetry part of entropy per particle (in terms of  $TS_{\text{sym}}/A$ ) of pure neutron matter at different temperatures, given by the CDM3Y3 and CDM3Y6 interactions [23, 39] and their soft CDM3Y3s and CDM3Y6s versions [8]. These two groups of the CDM3Yn interactions were shown in Fig. 4 to give very different behaviors of the free symmetry energy at high baryon densities. As can be seen in Fig. 13, the maximal  $TS_{\text{sym}}/A$  values associated with the stiff symmetry energy is slightly higher than that associated with the soft symmetry energy. However, the stiff-soft difference shown in Fig. 13 is not as drastic as that found in the free symmetry energy given by the CDM3Yn interactions and their soft versions at

different temperatures (see Fig. 4).

In conclusion, the different behaviors of entropy with the increasing baryon density shown in Figs. 10-12 is due to difference in the momentum dependence of single-particle potential used to construct the nucleon momentum distribution (5), the main input for the determination of entropy (12). This is also the source of difference in the nucleon effective mass obtained with different density dependent NN interactions shown in Figs. 7-8. In the same manner, a slight difference shown in Fig. 13 for the symmetry part of entropy per particle should be due to different the momentum dependences of the IV term of single-particle potential obtained with the CDM3Yn interactions and their soft CDM3Yns versions. This is directly related to the difference between the stiff- and soft symmetry-energy scenarios.

### III. EOS OF HOT $\beta$ -STABLE PNS MATTER

To study the  $\beta$ -stable hydrostatic configuration of PNS, one needs to keep the  $\beta$  equilibrium between  $n, p$  and  $e, \mu, \nu$ , and to combine the EOS of uniform matter in the core with an EOS of the hot PNS crust. We have considered, therefore, the EOS given by the RMF calculation by Shen *et al.* [7] (the improved version of 2011 [55]) for the PNS crust. The EOS of hot inhomogeneous PNS crust given by the RMF calculation was used for the baryon number densities up to the edge density  $n_{\text{edge}} \approx 0.05 \text{ fm}^{-3}$ , and the EOS of the uniform PNS matter given by our HF calculation has been used for  $n_b \gtrsim 0.08 \text{ fm}^{-3}$  following a brief transition region  $0.05 \lesssim n_b \lesssim 0.08 \text{ fm}^{-3}$  shown as dotted lines in Fig. 14. The energy and pressure in the transition region were determined by a spline procedure to ensure their smooth and continuous behavior from the inner crust to the uniform core. The transition density assumed in the present work is rather close to that found recently in a dynamical mean-field study of hot neutron star matter using the momentum-dependent effective interaction [56].

The uniform PNS core is assumed to be homogeneous matter of neutrons, protons, electrons, neutrinos, and muons ( $\mu^-$  appear at  $n_b$  above the muon threshold density, where electron chemical potential  $\mu_e > m_\mu c^2 \approx 105.6 \text{ MeV}$ ). In the present work, we have considered two different scenarios for neutrinos in the PNS matter:  $\nu$ -free (neutrinos are absent) and  $\nu$ -trapped (the PNS matter is opaque [2] and neutrinos are trapped inside the PNS). Thus, the total free energy density  $F$  of PNS matter is determined at the given baryon

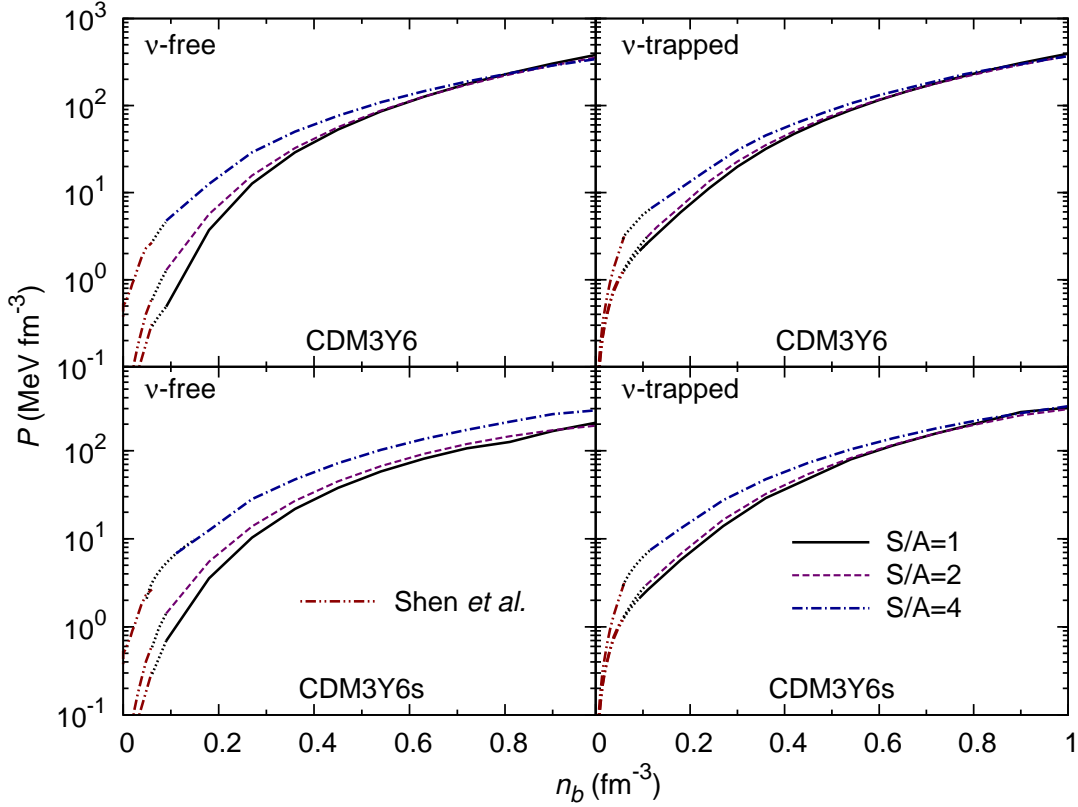


FIG. 14: Pressure (33) of the isentropic  $\nu$ -free (left panel) and  $\nu$ -trapped (right panel)  $\beta$ -stable PNS matter at different baryon densities  $n_b$  and entropy per baryon  $S/A = 1, 2$  and  $4$ . The EOS of the PNS crust is given by the RMF calculation by Shen *et al.* [7, 55], and the EOS of the uniform PNS core is given by the HF calculation using the CDM3Y6 interaction [39] (upper panel) and its soft CDM3Y6s version [8] (lower panel). The transition region matching the PNS crust with the uniform core is shown as the dotted lines.

number density  $n_b$  and temperature  $T$  as

$$F(T, n_b) = F_b(T, n_b) + F_l(T, n_b), \quad (24)$$

$$\text{where } F_b(T, n_b) = E_b(T, n_b) - TS_b(T, n_b), \quad (25)$$

$$E_b(T, n_b) = E(T, n_b) + n_n m_n c^2 + n_p m_p c^2, \quad (26)$$

$$\text{and } F_l(T, n_b) = \sum_{i=e,\mu,\nu} [E_i(T, n_b, n_i) - TS_i(T, n_b, n_i)]. \quad (27)$$

Here  $E(T, n_b)$  is the HF energy density of baryons (1) and  $S_b(T, n_b)$  is the corresponding baryon entropy density (12). The summation in (27) is done over all leptons under consideration, with the energy  $E_i$  and entropy  $S_i$  of the  $i$ -kind lepton evaluated in the relativistic



(non-interacting) Fermi gas model [6]. The EOS of PNS matter is usually discussed in terms of the total free energy per baryon and total entropy per baryon determined as

$$\frac{F(n_b, T)}{A} \equiv [F_b(n_b, T) + F_l(n_b, T)]/n_b \quad (28)$$

$$\frac{S(n_b, T)}{A} \equiv [S_b(n_b, T) + \sum_{i=e, \mu, \nu} S_i(n_b, n_i, T)]/n_b. \quad (29)$$

The chemical potentials of the constituent particles of PNS matter are constrained by the condition of  $\beta$ -equilibrium

$$\mu_n - \mu_p = \mu_e - \mu_{\nu_e} = \mu_\mu - \mu_{\nu_\mu}. \quad (30)$$

With the fraction of the  $k$ -kind constituent particle determined at the baryon number density  $n_b$  as  $x_k = n_k/n_b$ , the charge neutrality condition of  $\beta$ -stable PNS matter implies

$$x_p + \sum_{i=e, \mu, \nu} q_i x_i = 0, \quad (31)$$

where  $q_i$  is the charge of the  $i$ -kind lepton. The conservation of the weak charge leads to the conservation of the lepton fractions determined as

$$Y_l = x_l - x_{\bar{l}} + x_{\nu_l} - x_{\bar{\nu}_l}, \quad l = e, \mu. \quad (32)$$

Because of dynamical neutrino trapping during the core collapse [1], neutrinos are *trapped* during the first instants of the PNS [2, 11]. At the onset of neutrino trapping occurring at  $\rho_b \sim 10^{11} \text{g/cm}^3$  [61], the electron lepton fraction is expected to be  $Y_e \approx 0.4$  [11–13]. When the electron lepton fraction is fixed, the conversion of electrons to muons at high densities is unlikely and the muon lepton fraction can be assumed  $Y_\mu \approx 0$  [11, 12]. These assumptions for the  $\nu$ -trapped PNS matter, together with a chosen EOS for the baryon matter, are the constraints used to determine the  $npe\mu\nu$  composition of the  $\beta$ -stable,  $\nu$ -trapped PNS matter. In the  $\nu$ -free case, these conditions are simplified by setting all neutrino fractions to zero. We note that at very low baryon densities of  $n_b < 10^{-5} \text{fm}^{-3}$  neutrinos are no more trapped inside the dilute PNS atmosphere and become almost free [59]. We have chosen, therefore, also a “cut-off” procedure to impose the electron fraction  $x_e \approx 0.4$  at  $n_b \lesssim 10^{-5} \text{fm}^{-3}$  and the dilute PNS atmosphere is treated as  $\nu$ -free.

At zero temperature, a simple relation linking  $\mu_n - \mu_p$  and the nuclear symmetry energy based on the parabolic approximation (16) is often used to determine the proton, electron

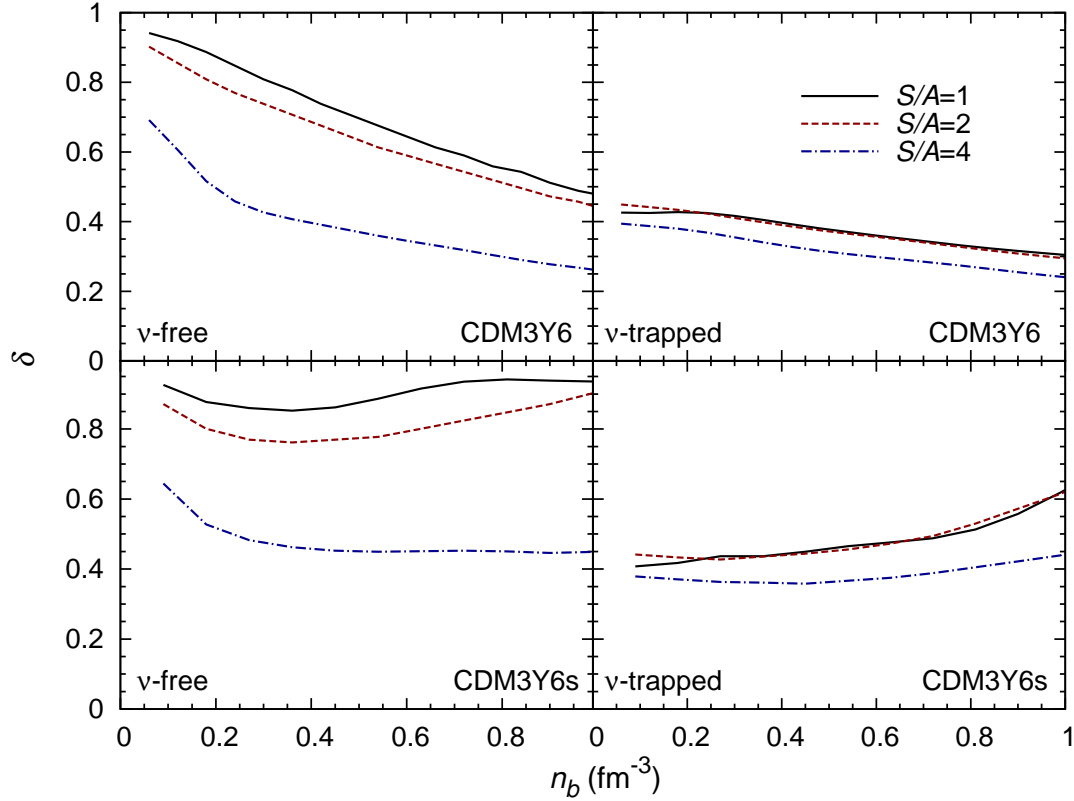


FIG. 15: Neutron-proton asymmetry  $\delta$  of the  $\nu$ -free (left panels) and  $\nu$ -trapped (right panels)  $\beta$ -stable PNS matter at different baryon number densities  $n_b$  and entropy per baryon  $S/A = 1, 2$  and 4. The EOS of the homogeneous PNS core is given by the HF calculation using the CDM3Y6 interaction [39] and its soft CDM3Y6s version [8].

and muon fractions of  $\beta$ -stable matter [8]. Because the parabolic approximation becomes poorer with the increasing temperature as shown in Sect. II, we avoid using it in the present HF calculation. Thus, at each temperature  $T$  the EOS associated with a given effective NN interaction is first constructed in a dense grid of the neutron-proton asymmetries  $\delta$  and baryon number densities  $n_b$ . Then, at the given temperature and baryon density, the actual asymmetry parameter  $\delta$  is obtained by ensuring the conditions of  $\beta$ -equilibrium (24), charge neutrality (31) and lepton number conservation (32). At each step of this variation procedure, the chemical potentials of constituent particles are determined by normalizing the Fermi-Dirac momentum distribution to the corresponding number density at the given  $T$ ,  $n_b$ , and  $\delta$ . With the obtained PNS composition, the temperature dependent EOS of  $\beta$ -stable  $npe\mu\nu$  matter is fully given by the total free energy density  $F(T, n_b)$  determined by

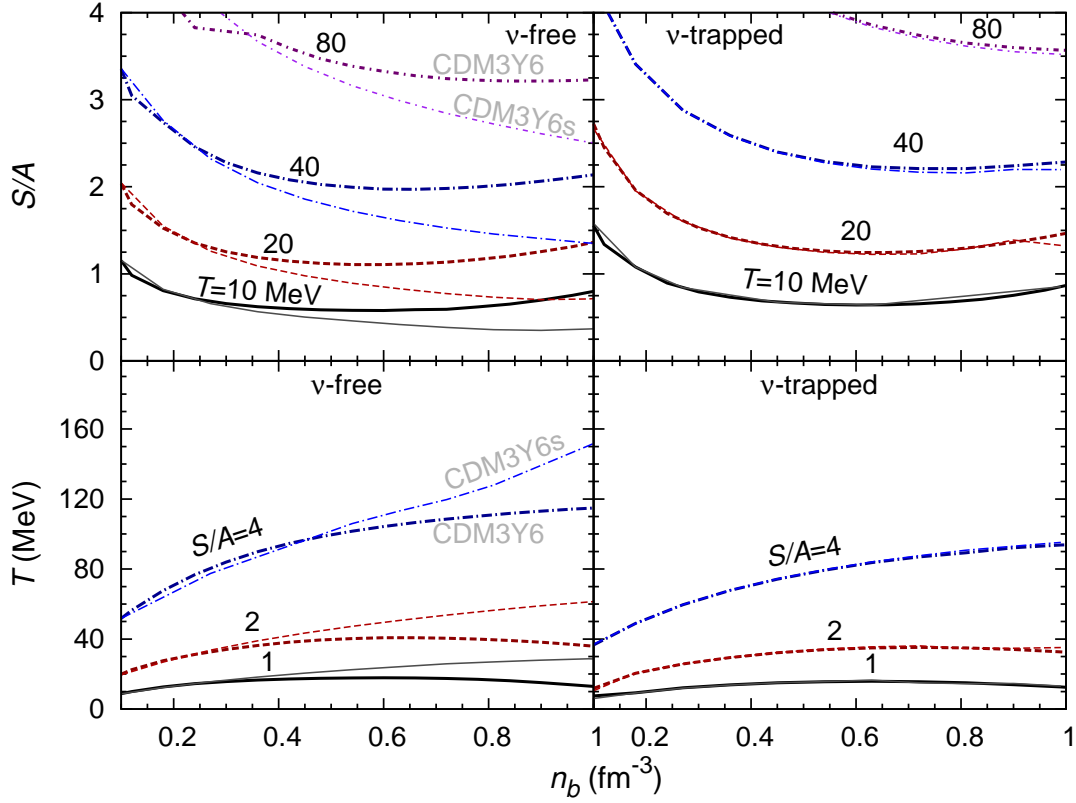


FIG. 16: (Color online) Entropy per baryon (upper panel) and temperature (lower panel) as function of baryon number density  $n_b$  of the  $\beta$ -stable PNS matter given by the CDM3Y6 interaction [23, 39] (thick lines) and its soft CDM3Y6s version [8] (thin lines) in the  $\nu$ -free (left panel) and  $\nu$ -trapped (right panel) cases.

Eq. (24) and total pressure  $P(T, n_b)$  determined as

$$P(T, n_b) = n_b^2 \frac{\partial}{\partial n_b} \left[ \frac{F_b(T, n_b)}{n_b} \right] + \sum_{i=e,\mu,\nu} P_i(T, n_b, n_i). \quad (33)$$

Like the lepton internal energy  $E_i$ , the pressure of the  $i$ -kind lepton  $P_i$  is also determined by the relativistic free Fermi gas model [6]. The total entropy density  $S(T, n_b)$  at each baryon density was also determined in a dense grid of different temperatures  $T$ , so that the isentropic behavior of all considered thermodynamic quantities can be easily interpolated at different baryon densities. For example, the total pressure  $P$  representing the EOS of the isentropic,  $\nu$ -free and  $\nu$ -trapped  $\beta$ -stable matter is shown in Fig. 14. One can see that the difference between the soft- and stiff symmetry energy scenarios is quite significant in the  $\nu$ -free case, while it becomes somewhat weaker for the  $\nu$ -trapped PNS matter.

At variance with the HF calculation of NM, the neutron-proton asymmetry  $\delta$  in the  $\beta$ -stable PNS matter becomes a thermodynamic quantity, determined consistently by the (equilibrated) neutron and proton fractions at temperature  $T$  and baryon number density  $n_b$ . The  $\delta$  values given by the HF calculation using the CDM3Y6 and CDM3Y6s interactions for the isentropic  $\beta$ -stable  $npe\mu\nu$  matter at the total entropy per baryon  $S/A = 1, 2$  and 4 are shown in Fig. 15. One can see that for both the stiff- and soft symmetry-energy scenarios, the hot PNS matter with high entropy of  $S/A = 4$  becomes more proton rich compared to that at the lower temperature or entropy. In the  $\nu$ -free case (see left panel of Fig. 15), the  $\delta$  value given by the stiff CDM3Y6 interaction at  $S/A = 1, 2$  decreases gradually from about 0.9 at low densities to around 0.5 at  $n_b = 1 \text{ fm}^{-3}$ . The same trend was found at  $S/A = 4$ , but the matter is more symmetric or more proton rich. The behavior of  $\delta$  value given by the soft CDM3Y6s interaction at entropy  $S/A = 1, 2$  is similar to that found earlier [8] for the  $\beta$ -stable matter at zero temperature, with the core matter remaining very neutron rich over the whole density range. As temperature increases to the thermal equilibrium at  $S/A = 4$ , the difference between the two scenarios for the symmetry energy becomes less sizable and  $\delta$  value decreases to around 0.25-0.45 at the highest baryon density. The neutrino trapping was found to make the difference between the stiff and soft symmetry-energy scenarios less significant (see right panel of Fig. 15), with the matter becoming more proton rich over a wide range of baryon densities. Such an enhancement of the proton fraction in PNS matter by neutrino trapping was also found in the BHF calculation by Vidaña *et al.* [57] that includes hyperons. The suppression of the impact of the nuclear symmetry energy in the presence of trapped neutrinos is mainly explained by the fact that the PNS matter is more symmetric and weak processes, like  $p + e^- \leftrightarrow n + \nu_e$ , can proceed in both directions. It is clearly seen in Fig. 15 that the more symmetric matter the less impact of the symmetry energy. This effect is also illustrated in the density profiles of entropy and temperature of the  $\beta$ -stable PNS matter given by the CDM3Y6 and CDM3Y6s interactions shown in Fig. 16. One can see on the left panel of Fig. 16 that in the  $\nu$ -free case, the difference between the stiff and soft symmetry-energy scenarios is strongest at high baryon densities so that the center of PNS becomes much hotter when the symmetry energy is soft. Such an impact to the density profiles of entropy and temperature by the symmetry energy is, however, suppressed in the presence of trapped neutrinos (see right panel of Fig. 16).

Beside the symmetry energy, the impact of nucleon effective mass to the thermal prop-

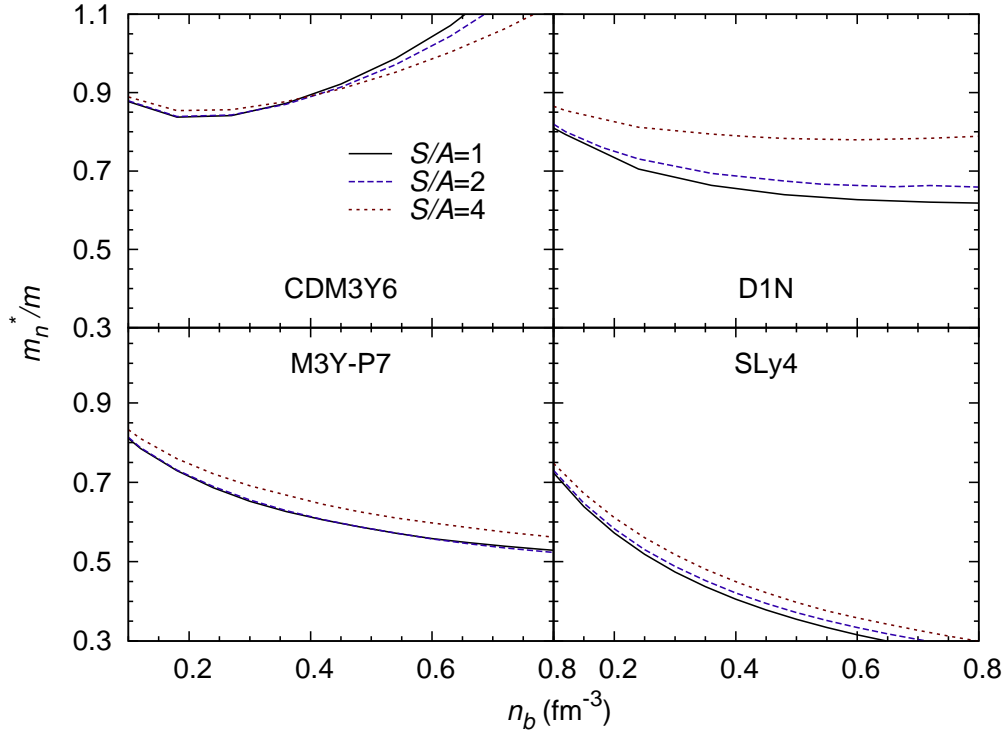


FIG. 17: (Color online) Density profile of neutron effective mass in the  $\nu$ -free and  $\beta$ -stable PNS matter at entropy per baryon  $S/A = 1, 2$  and  $4$ , given by the HF calculation using the CDM3Y6 [39] and M3Y-P7 [28] interactions (left panel), the D1N version of Gogny interaction [30] (right panel) and SLy4 version [32] of Skyrme interaction (right panel).

erties of NM was found quite significant in the previous section, and it is of interest to explore the effect of  $m_\tau^*$  in the  $\beta$ -stable PNS matter at different temperatures and entropy. The density profiles of neutron and proton effective masses in the  $\nu$ -free and  $\beta$ -stable PNS matter at entropy per baryon  $S/A = 1, 2$  and  $4$ , obtained with different density dependent NN interactions are shown in Figs. 17 and 18. One can see that the density dependence of nucleon effective mass in the hot  $\beta$ -stable PNS matter is quite similar to that at zero temperature shown in Figs. 7 and 8. While nucleon effective mass given by the CDM3Y6 interaction saturates at  $n_b \approx 0.2 \text{ fm}^{-3}$  and rises up to above unity at high baryon densities (in agreement with the BHF calculation [52] that includes 3-body forces), the  $m_\tau^*$  values given by other interactions steadily decrease with the increasing baryon density. The fall of nucleon effective mass given by the M3Y-P7 and Sly4 interactions is very drastic at high densities and it should result, therefore, on very high temperature in the center of PNS. The density profiles of temperature in the  $\nu$ -free and  $\beta$ -stable PNS matter at entropy per

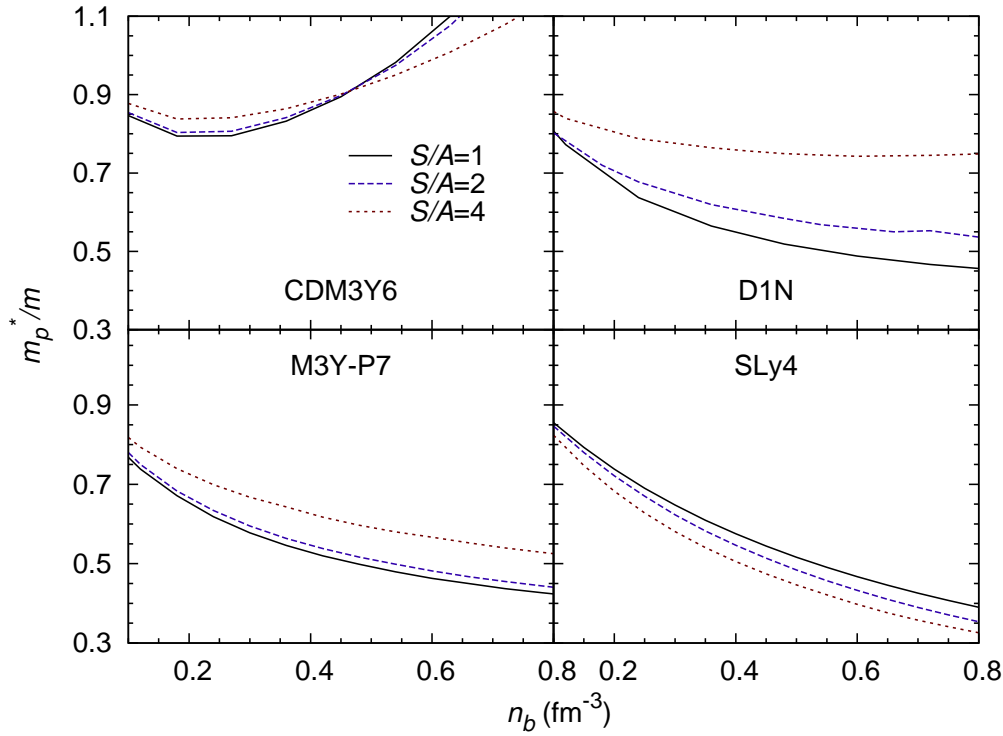


FIG. 18: (Color online) The same as Fig. 17 but for proton effective mass.

baryon  $S/A = 1, 2$  and  $4$ , given by the same density dependent NN interactions are shown in Fig. 19. It can be seen that the rise of temperature with the increasing baryon density given by the M3Y-P7 and Sly4 interactions is indeed very stiff, to  $T$  above 200 MeV at high densities. We will see below that such different behaviors of nucleon effective mass also influence strongly the hydrostatic configuration of hot PNS.

Based on different EOS's given by different density dependent NN interactions, the composition of the  $\beta$ -stable PNS in terms of the constituent-particle fractions at entropy per baryon  $S/A = 1, 2$  and  $4$  is quite different (see Figs. 20-23). The results shown in Figs. 20 and 22 were obtained for the  $\nu$ -free PNS matter that corresponds the late stage of the evolution of PNS when most of neutrinos have escaped from the core. In this case the difference between the stiff- and soft symmetry-energy scenarios is quite significant as discussed above for the neutron-proton asymmetry. A comparison with the BHF results obtained for the  $\beta$ -stable PNS matter at entropy  $S/A = 1, 2$  (see upper panels of Figs. 20 and 22, and Fig. 4 of Ref. [12]) shows that the asy-stiff interactions (CDM3Y3, CDM3Y6, and SLy4) give the results rather close to the BHF results, while the results given by the asy-soft interactions (CDM3Y3s, CDM3Y6s, and M3Y-P7) are very different from the BHF results. The results

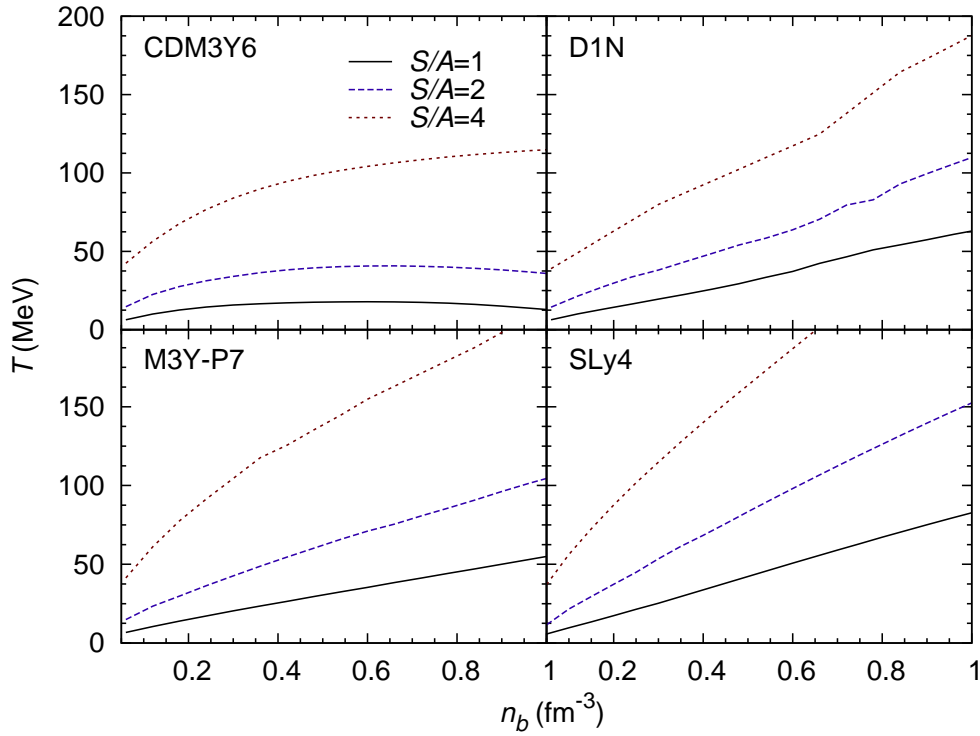


FIG. 19: (Color online) Density profile of temperature in the  $\nu$ -free and  $\beta$ -stable PNS matter at entropy per baryon  $S/A = 1, 2$  and  $4$ , deduced from the HF results obtained with the same density dependent NN interactions as those considered in Fig. 17.

shown in Figs. 21 and 23 were obtained for the  $\nu$ -trapped PNS matter with the electron lepton fraction  $Y_e \approx 0.4$ , as expected during the first stage of the core-collapse supernovae [11–13]. In such a scenario, the electron conversion to muon is unlikely at low temperatures or entropy, and the muon fraction was found much suppressed at  $S/A = 1$  and  $2$ . At high temperatures of the PNS matter at  $S/A = 4$ , the electron chemical potential  $\mu_e$  increases and exceeds the muon threshold, and muons appear again.

In both cases, the effect of the symmetry energy is clearly demonstrated: at high baryon densities, the asy-stiff interactions always give higher electron and proton fractions compared with those given by the asy-soft interactions. Such an impact of the symmetry energy is more pronounced in the  $\nu$ -free case, where the electron fraction  $x_e$  predicted by the asy-soft models reduces significantly to below  $0.1$  at high baryon densities. As discussed in Ref. [8], the difference in the electron fraction caused by different slopes of the symmetry energy at high baryon densities has a drastic effect on the  $\nu$ -emission process during the cooling of neutron star. Namely, in the soft symmetry-energy scenario, the direct Urca process is

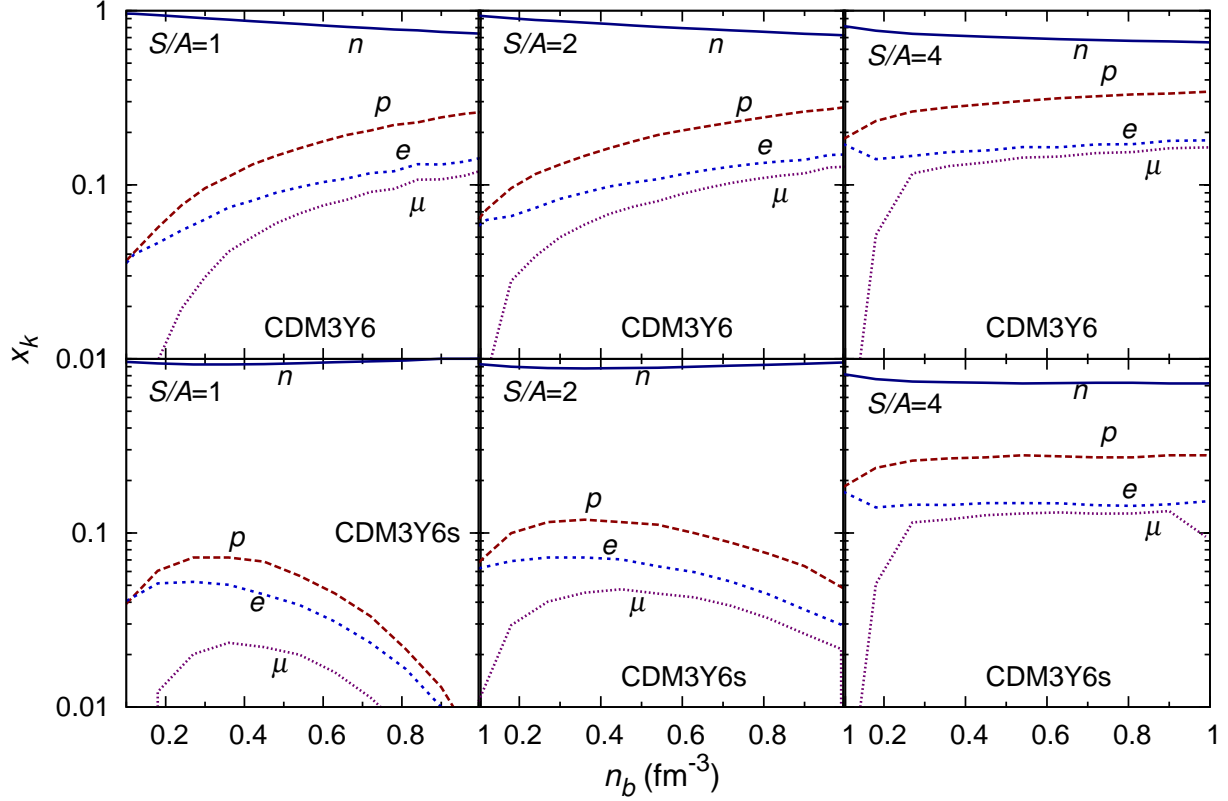


FIG. 20: (Color online) Particle fractions as function of baryon number density  $n_b$  in the  $\nu$ -free and  $\beta$ -stable PNS matter at entropy per baryon  $S/A = 1, 2$  and  $4$ , given by the CDM3Y6 interaction [39] (upper panel) and its soft CDM3Y6s version [8] (lower panel).

strongly quenched because of  $Y_e < 11\%$  [8, 60], while it is well allowed in the stiff symmetry-energy scenario. The difference in the electron fraction caused by different slopes of the symmetry energy is less pronounced in very hot PNS matter at  $S/A = 4$ . Such state of hot PNS matter has been shown to occur at the onset of collapse of a very massive ( $40 M_\odot$ ) progenitor to black hole [9, 10].

It is interesting to note the difference between results obtained in the  $\nu$ -trapped and  $\nu$ -free cases. Although  $\beta$ -equilibrium implies the weak processes  $l + p \leftrightarrow n + \nu_l$ , in the  $\nu$ -free PNS matter most of neutrinos have escaped and cannot contribute to these processes, and they proceed preferably in one direction (from left to right). As a result, the PNS matter undergoes the neutronization process [1, 63]. Therefore, the  $\nu$ -free PNS matter is always more neutron-rich than the  $\nu$ -trapped matter as shown above in Fig. 15. Finally we discuss also the effect of increasing temperature (or equivalently increasing entropy) on the particle



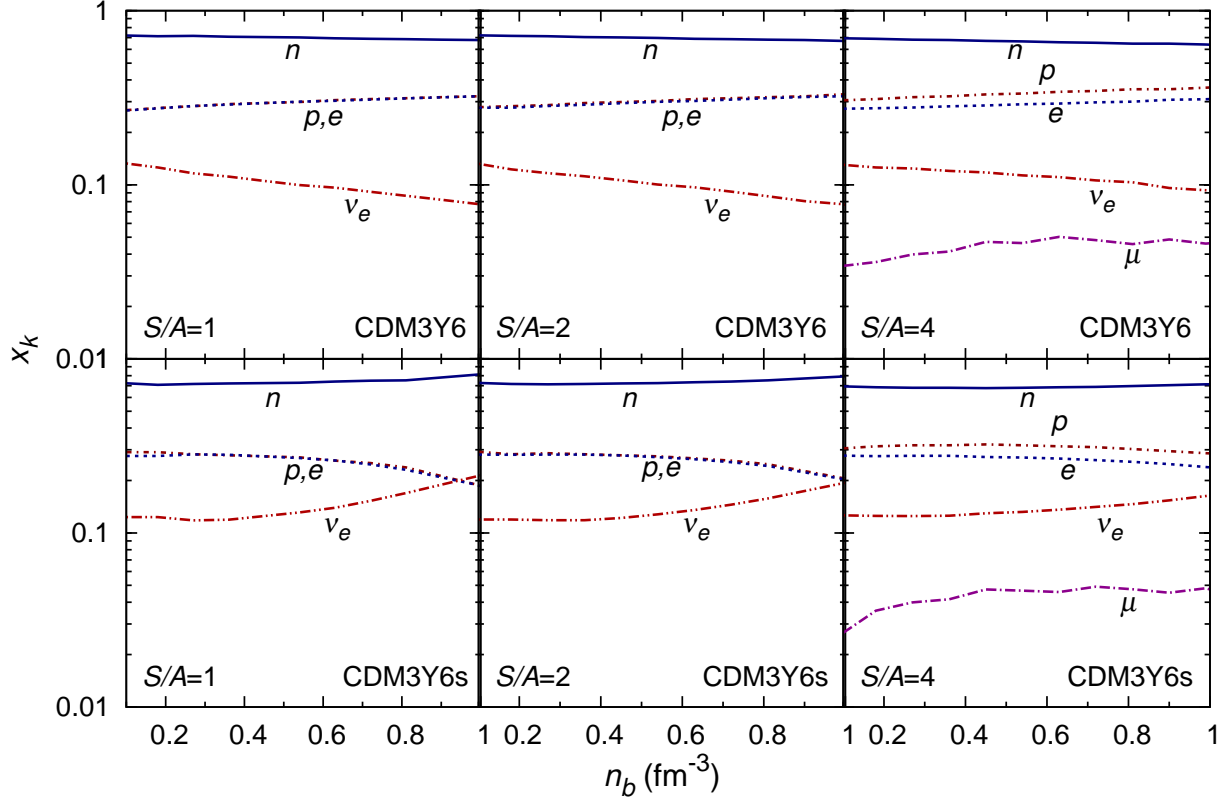


FIG. 21: The same as Fig. 20 but for the  $\nu$ -trapped,  $\beta$ -stable matter of the PNS.

fractions shown in Figs. 20-23. In general, the increase of temperature tends to reduce the difference between the neutron and proton fractions ( $n_n$  decreases while  $n_p$  increases with  $T$ ). In a similar way, the difference between  $e$  and  $\mu$  becomes also less pronounced with the increasing temperature ( $n_e$  decreases and  $n_\mu$  increases with  $T$ ). Such a phenomenon is expected to occur between particles of similar nature, and the hot matter tends to quench the difference in their masses. Although the impact of the symmetry energy in the presence of trapped neutrinos was shown to be less significant with increasing entropy, we found that the symmetry energy still has some effect on the neutrino fraction in the high-density  $\nu$ -trapped PNS matter at  $S/A = 4$ . Even with a fixed electron lepton fraction  $Y_e = 0.4$ , the neutrino fraction  $x_\nu < 10\%$  was found with the asy-stiff CDM3Y6 interaction as  $n_b$  approaches  $1 \text{ fm}^{-3}$ , while  $x_\nu$  close to  $20\%$  was found with the soft CDM3Y6s interaction (see right panel of Fig. 21). The result given by the stiff CDM3Y6 interaction seems to agree well with those of the recent hydrodynamic simulation of black hole formation in the failed core-collapse supernova [9], which suggested that the thermodynamic condition of hot  $\beta$ -

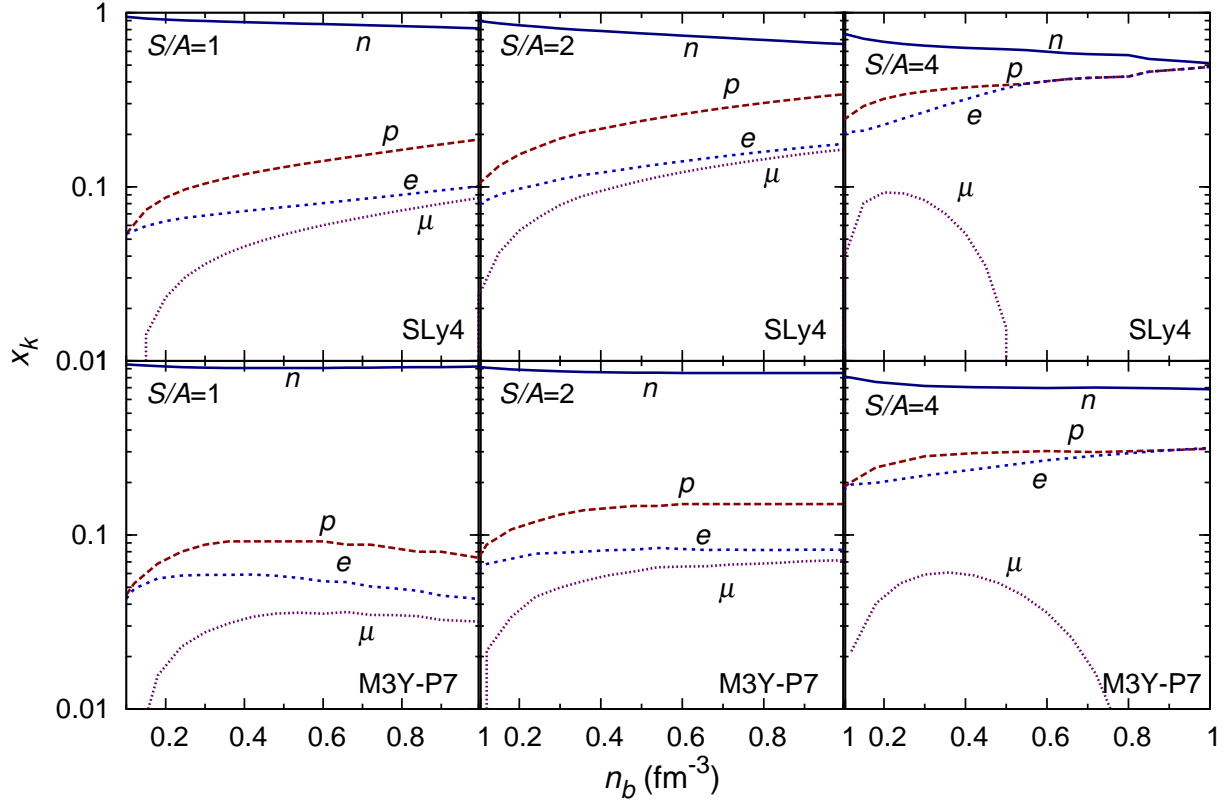


FIG. 22: (Color online) The same as Fig. 20, but given by the SLy4 version [32] of Skyrme interaction (upper panel) and M3Y-P7 interaction parametrized by Nakada [28] (lower panel).

stable PNS matter at the onset of collapse of a massive ( $40 M_{\odot}$ ) progenitor to black hole can be approximated by a constant entropy per baryon  $S/A \approx 4$ , with a *negligible* contribution of neutrinos ( $Y_{\nu_e} + Y_{\bar{\nu}_e} < 0.05$  at  $0.2 < Y_e < 0.3$  as shown in Fig. 16 of Ref. [9]).

#### IV. $\beta$ -STABLE CONFIGURATION OF HOT PROTONEUTRON STAR

We used the total internal energy  $E$  and pressure  $P$  inside PNS at entropy per baryon  $S/A = 1, 2$  and  $4$  given by the different EOS's discussed above in Sec. III as inputs for the Tolman-Oppenheimer-Volkov (TOV) equations [6]. The  $\beta$ -stable hydrostatic configuration of hot PNS in different scenarios given by the solutions of the TOV equations are presented in Tables II and III, and Figs. 24-26. For comparison, we have also presented in these tables the  $\beta$ -stable configuration of cold ( $\nu$ -free) neutron star, given by the solutions of the TOV equations obtained with the same EOS's [8].

As was done at zero temperature [8], in order to explore explicitly the effects caused

TABLE II: Properties of the  $\nu$ -free and  $\nu$ -trapped,  $\beta$ -stable PNS at entropy per baryon  $S/A = 1, 2$  and 4, given by the solutions of the TOV equations using the EOS's based on the CDM3Y3, CDM3Y6 interactions [39] and their soft CDM3Y3s, CDM3Y6s versions [8].  $M_{\max}$  and  $R_{\max}$  are the maximum gravitational mass and radius;  $n_c$ ,  $\rho_c$ ,  $P_c$ , and  $T_c$  are the baryon number density, mass density, total pressure, and temperature in the center of PNS.  $T_s$  is temperature of the outer core of PNS, at baryon density  $\rho_s \approx 0.63 \times 10^{15}$  g/cm<sup>3</sup>. Results at  $S/A = 0$  represent the stable configuration of cold ( $\nu$ -free) neutron star [8].

EOS	$S/A$	$M_{\max}$ ( $M_{\odot}$ )	$R_{\max}$ (km)	$n_c$ (fm <sup>-3</sup> )	$\rho_c$ ( $10^{15}$ g/cm <sup>3</sup> )	$P_c$ (MeV fm <sup>-3</sup> )	$T_c$ (MeV)	$T_s$ (MeV)
CDM3Y3 ( $\nu$ -free)	0	1.59	9.70	1.44	3.16	494.4	0.0	
	1	1.64	9.60	1.53	3.16	538.9	19.7	17.6
	2	1.65	10.14	1.40	2.90	446.8	49.4	37.9
	4	1.94	14.67	0.78	1.58	180.5	113.6	84.6
CDM3Y3 ( $\nu$ -trapped)	1	1.67	10.59	1.44	2.90	470.8	18.7	14.3
	2	1.69	11.40	1.29	2.59	373.9	44.7	30.1
	4	1.99	15.67	0.75	1.45	163.1	91.4	66.9
CDM3Y3s ( $\nu$ -free)	0	1.13	9.36	1.61	3.26	261.1	0.0	
	1	1.18	9.53	1.52	3.07	253.0	37.4	18.4
	2	1.33	10.47	1.30	2.66	239.0	71.4	39.0
	4	1.93	15.28	0.67	1.33	130.6	120.3	86.1
CDM3Y3s ( $\nu$ -trapped)	1	1.55	10.84	1.46	2.90	390.3	18.0	14.2
	2	1.58	11.31	1.30	2.59	319.0	46.5	30.1
	4	1.93	14.91	0.77	1.50	161.8	91.5	69.0
CDM3Y6 ( $\nu$ -free)	0	1.95	10.23	1.20	2.74	627.3	0.0	
	1	1.97	10.25	1.24	2.73	626.5	10.1	17.4
	2	1.93	10.68	1.18	2.59	524.1	33.7	37.5
	4	2.12	14.37	0.80	1.63	235.5	114.1	86.8
CDM3Y6 ( $\nu$ -trapped)	1	2.03	11.11	1.18	2.51	553.9	9.7	18.3
	2	2.00	11.46	1.13	2.37	467.7	24.8	29.6
	4	2.11	14.29	0.82	1.68	246.6	89.7	66.6
CDM3Y6s ( $\nu$ -free)	0	1.42	9.74	1.46	3.06	340.4	0.0	
	1	1.65	9.20	1.50	3.45	652.7	17.1	18.3
	2	1.37	11.13	1.16	2.44	212.9	65.4	38.8
	4	1.96	14.24	0.80	1.67	206.9	121.5	84.5
CDM3Y6s ( $\nu$ -trapped)	1	2.04	11.67	1.02	2.02	314.7	12.3	13.9
	2	1.88	11.68	1.12	2.30	353.9	34.6	29.8
	4	2.06	14.24	0.84	1.68	229.4	91.2	66.7

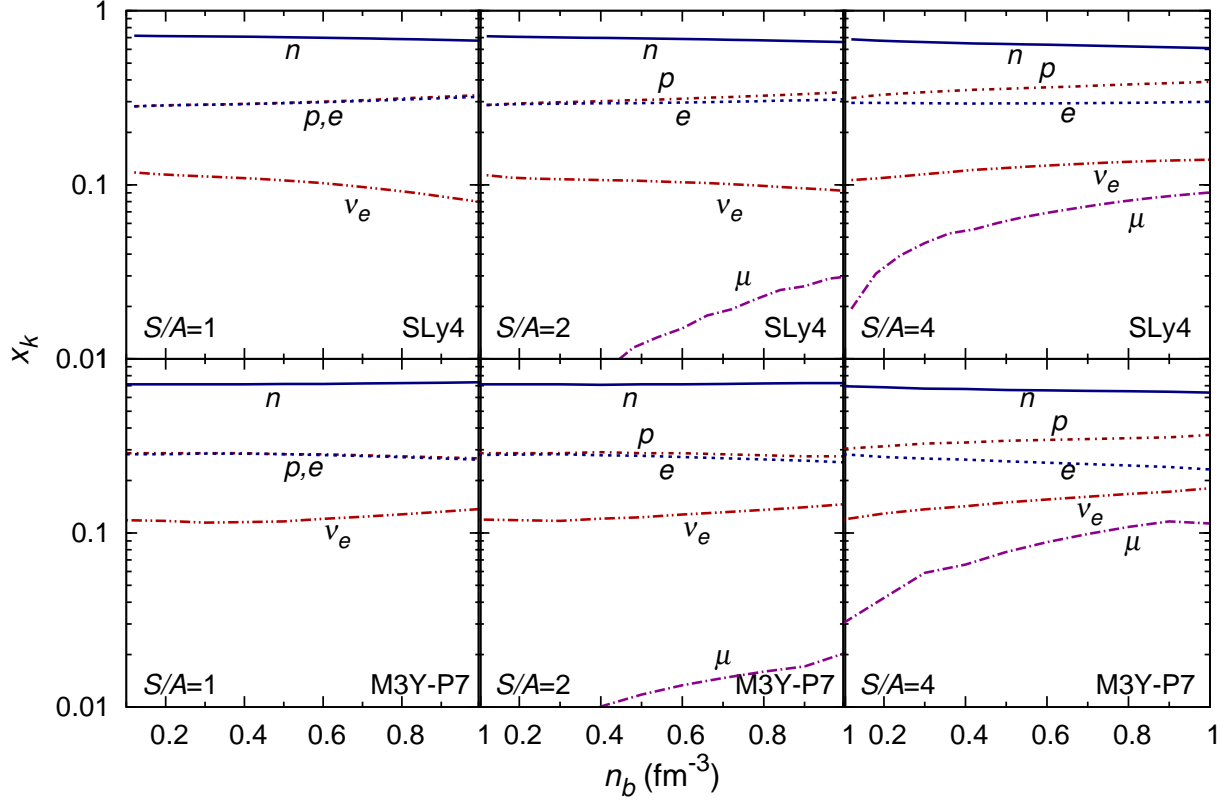


FIG. 23: The same as Fig. 22 but for the  $\nu$ -trapped,  $\beta$ -stable PNS matter.

by the nuclear symmetry energy to the stable configuration of PNS, we have considered solutions of the TOV equations given by the EOS's based on the CDM3Y3 and CDM3Y6 interactions [39] and their soft versions CDM3Y3s and CDM3Y6s [8]. The only difference between these two groups of the CDM3Yn interaction is the modeling of the IV density dependence that gives different slopes of the free symmetry energy at high NM densities and different temperatures as shown in Fig. 4. One can see in Tables II and Figs. 24 and 25 that in the  $\nu$ -free case, the impact of the symmetry energy is quite strong at entropy per baryon  $S/A = 0, 1$  and  $2$ . For example, the PNS maximum gravitational mass obtained with the CDM3Y3s interaction at  $S/A = 1$  is  $M_{\max}(\text{CDM3Y3s}) \approx 1.18 M_{\odot}$ , and it increases to  $M_{\max}(\text{CDM3Y3}) \approx 1.64 M_{\odot}$  when the density dependence of the symmetry energy is changed from the soft to the stiff behavior. Similarly with the CDM3Y6 interaction, we found  $M_{\max}(\text{CDM3Y6s}) \approx 1.65 M_{\odot}$  and  $M_{\max}(\text{CDM3Y6}) \approx 1.97 M_{\odot}$  at  $S/A = 1$  (see Fig. 24). Thus, the difference in the slope of the symmetry energy at high NM densities could lead to a difference of  $0.3 - 0.5 M_{\odot}$  in the predicted  $M_{\max}$  value. We note further that

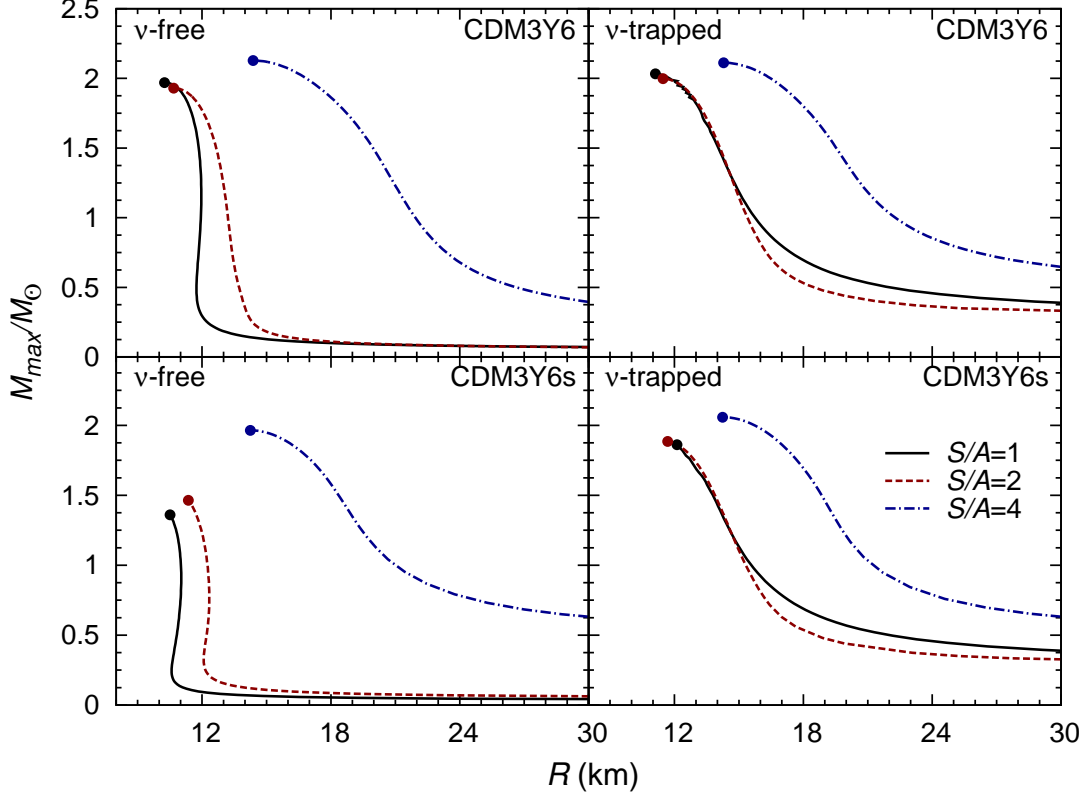


FIG. 24: (Color online) Gravitational mass (in unit of solar mass  $M_\odot$ ) of the  $\beta$ -stable,  $\nu$ -free (left panel) and  $\nu$ -trapped (right panel) PNS at entropy  $S/A = 1, 2$  and  $4$  as function of the radius (in km), based on the EOS of the homogeneous PNS core given by the CDM3Y6 interaction [39] (upper panel) and its soft CDM3Y6s version [8] (lower panel). The circle at the end of each curve indicates the last stable configuration.

$M_{\max}$  obtained with the CDM3Y6 interaction at  $S/A = 0, 1$  is quite close to the neutron star mass of  $1.97 M_\odot$  observed recently by Demores *et al.* [58]. Because the isospin dependences of the CDM3Y3 and CDM3Y6 interactions are nearly the same, the difference of about  $0.3 M_\odot$  in the  $M_{\max}$  values at  $S/A = 0, 1$  obtained with these two interactions in the  $\nu$ -free case should be due to different nuclear incompressibilities  $K_0$  (see Table I). Concerning other NN interactions under study, only the Sly4 and M3Y-P7 interactions give the  $M_{\max}$  values at  $S/A = 0, 1$  close to the observed neutron star mass of  $1.97 M_\odot$  [58]. The D1N interaction gives a too low  $M_{\max} \approx 1.23$  and  $1.32 M_\odot$  at  $S/A = 0$  and  $1$ , respectively, while the M3Y-P5 interaction gives unstable results for the PNS configuration at high temperatures and baryon densities, and are not included in the present discussion. We note that the instability of the

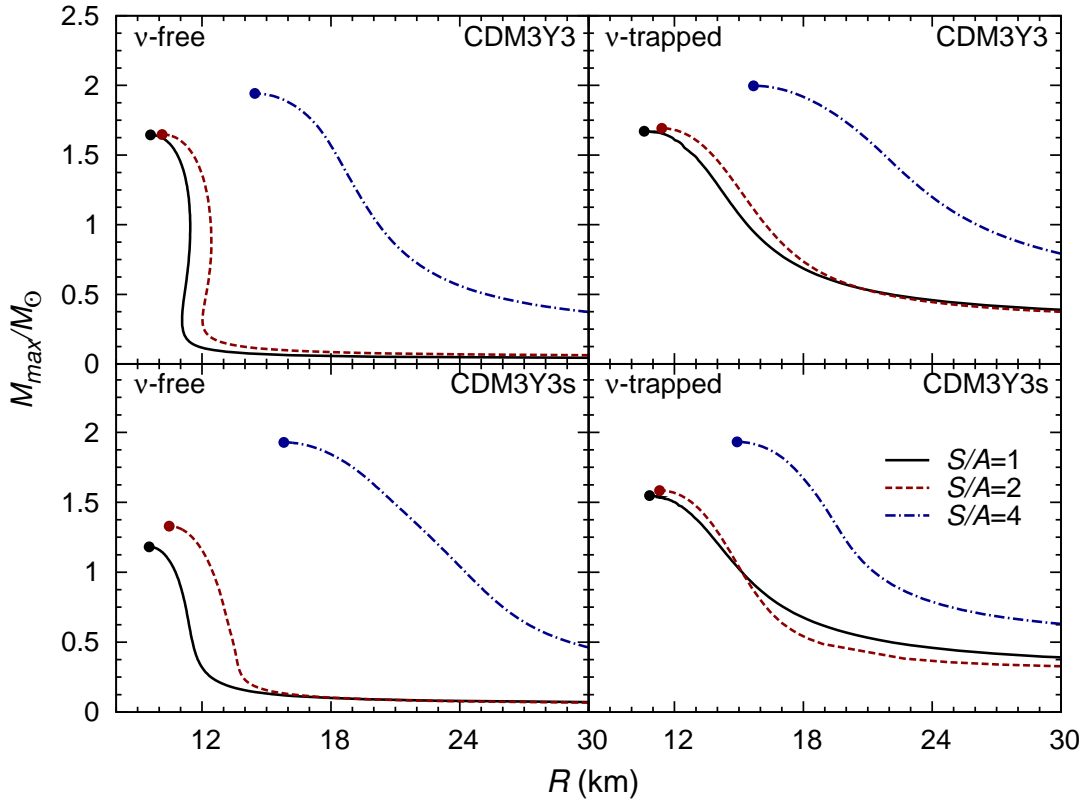


FIG. 25: The same as Fig. 24 but given by the CDM3Y3 interaction [39] (upper panel) and its soft CDM3Y3s version [8] (lower panel).

results given by the M3Y-P5 interaction is purely numerical one that is likely due to the parametrization of this version of M3Y-Pn interaction.

In the presence of trapped neutrinos, the effect caused by different slopes of the symmetry energy is diminished already at entropy  $S/A = 1$  and 2, and stable values of the maximum mass and radius of PNS are rather close, independent of the behavior of the symmetry energy (see Tables II, Figs. 24 and 25). We note that the microscopic BHF calculation of the  $\nu$ -trapped, isentropic PNS [12] gives the maximum mass  $M_{\max} \approx 1.95 M_{\odot}$  at entropy per baryon  $S/A = 1$  and 2, and the corresponding  $R_{\max} \approx 10.3$  and 10.8 km. Thus, only the PNS configuration obtained with the CDM3Y6 interaction has the maximum mass close to the BHF result, while the maximum radius is slightly larger than that predicted by the BHF calculation.

At much higher temperatures of the PNS matter at  $S/A = 4$ , the impact of the symmetry energy becomes weaker and similar  $\beta$ -stable configurations were found with both the asy-stiff

TABLE III: The same as Table II but obtained with the EOS's based on the SLy4 version [32] of Skyrme interaction, M3Y-P7 interaction parametrized by Nakada [28], and D1N version [30] of Gogny interaction.

EOS	$S/A$	$M_{\max}$ ( $M_{\odot}$ )	$R_{\max}$ (km)	$n_c$ ( $\text{fm}^{-3}$ )	$\rho_c$ ( $10^{15}\text{g}/\text{cm}^3$ )	$P_c$ ( $\text{MeV fm}^{-3}$ )	$T_c$ (MeV)	$T_s$ (MeV)
SLy4 ( $\nu$ -free)	0	2.05	9.96	1.21	2.86	860.4	0.0	
	1	2.06	10.07	1.18	2.74	776.3	96.2	30.4
	2	2.11	10.66	1.08	2.51	666.3	162.9	61.9
	4	2.37	14.60	0.70	1.54	279.8	214.0	122.6
SLy4 ( $\nu$ -trapped)	1	2.16	11.00	1.13	2.51	717.7	56.2	19.5
	2	2.16	11.16	1.10	2.44	661.9	92.1	41.1
	4	2.14	12.07	1.03	2.30	564.9	148.9	81.9
M3Y-P7 ( $\nu$ -free)	0	2.07	10.05	1.17	2.82	869.9	0.0	
	1	2.14	10.23	1.13	2.66	827.6	60.9	23.5
	2	2.23	11.09	1.00	2.00	645.8	104.9	48.09
	4	2.40	13.86	0.75	1.73	365.3	174.8	109.5
M3Y-P7 ( $\nu$ -trapped)	1	2.15	10.49	1.14	2.73	999.7	42.7	16.1
	2	2.22	11.09	1.07	2.44	738.9	75.7	38.0
	4	2.27	11.68	1.05	2.30	693.0	138.8	77.2
D1N ( $\nu$ -free)	0	1.23	7.75	2.36	5.24	819.9	0.0	
	1	1.32	8.46	1.88	4.10	581.3	97.9	22.8
	2	1.61	10.31	1.29	2.82	389.3	139.9	43.1
	4	2.22	14.28	0.77	1.67	282.9	148.9	84.7
D1N ( $\nu$ -trapped)	1	1.82	12.20	1.07	2.05	249.5	32.8	15.1
	2	1.96	12.22	1.06	2.11	314.1	64.0	31.0
	4	2.28	14.28	0.85	1.77	352.6	103.0	66.5

and asy-soft interactions in both the  $\nu$ -free and  $\nu$ -trapped scenarios. However, the effect of the increasing entropy on the maximum gravitational mass and radius of the  $\beta$ -stable PNS is very significant, and we found a strong increase of  $M_{\max}$  and  $R_{\max}$  at entropy per baryon  $S/A = 4$  compared to those obtained at  $S/A = 0$  (see Tables II and III, and Figs. 24-26). The hot PNS at  $S/A = 4$  is substantially expanded in its mass ( $\Delta M_{\max} \approx 0.3 - 0.5 M_{\odot}$ ) and size ( $\Delta R_{\max} \approx 4 - 5$  km), while the pressure in the core is decreased by a factor up to three. The case of the D1N interaction is extreme with the differences  $\Delta M_{\max} \approx 1 M_{\odot}$  and  $\Delta R_{\max} \approx 6.5$  km found between the cold neutron star and hot PNS at  $S/A = 4$  (both being in  $\beta$ -equilibrium without trapped neutrinos).

With a minor impact of the symmetry energy at entropy  $S/A = 4$ , a very substantial dif-

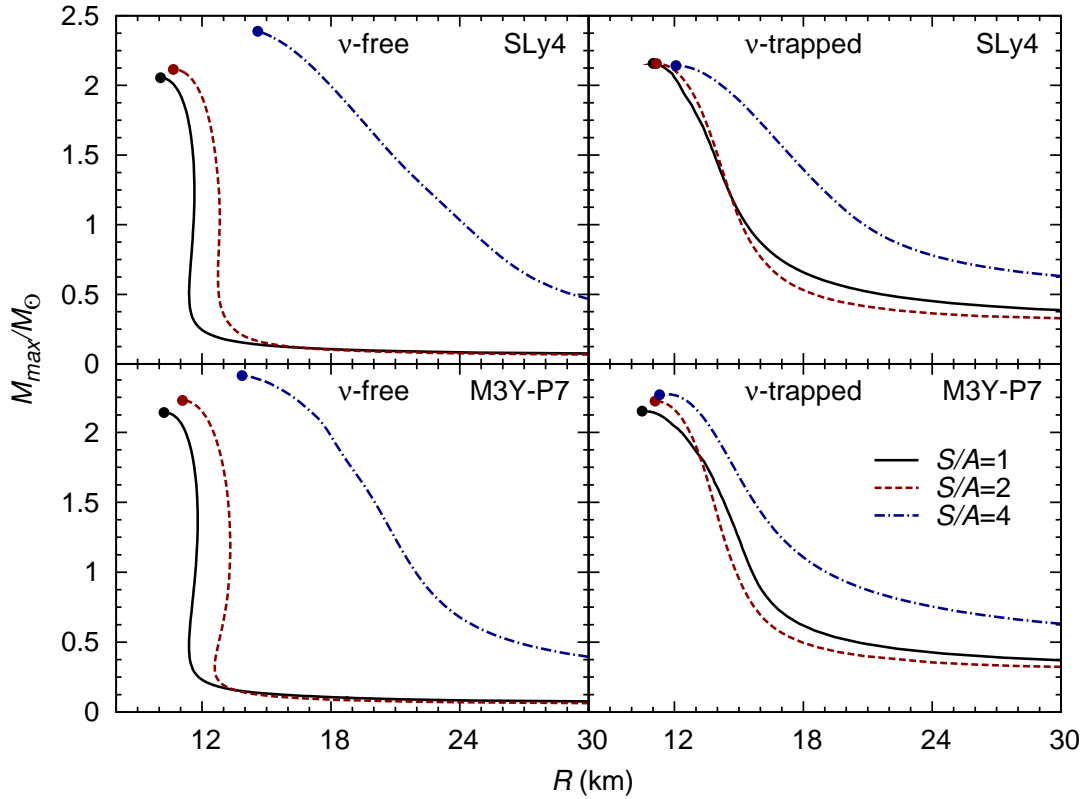


FIG. 26: The same as Fig. 24 but given by the SLy4 version of Skyrme interaction [32] (upper panel) and M3Y-P7 interaction parametrized by Nakada [28] (lower panel).

ference in temperature of hot PNS matter given by different density dependent interactions (shown in the last two columns of Tables II and III) is directly related to the difference in nucleon effective mass illustrated in Figs. 17-19. While the maximum gravitational masses obtained with the D1N, M3Y-P7 and Sly4 interactions are only slightly larger than that obtained with the CDM3Y6 interaction by  $\Delta M_{\text{max}} \approx 0.1 M_{\odot}$ , the difference in temperature of PNS at entropy  $S/A = 4$  is very large, up to about 100 MeV. The recent hydrodynamic simulation of the gravitational collapse of a massive  $40 M_{\odot}$  protoneutron progenitor to black hole [9] has shown that the  $\beta$ -stable matter (with very small neutrino fraction) in the outer core of PNS, is reaching  $S/A \approx 4$  at baryon density  $\rho_s \approx 0.63 \times 10^{15} \text{ g/cm}^3$  and temperature  $T_s \approx 80 - 90 \text{ MeV}$ , depending on the inputs of the EOS of  $\beta$ -stable PNS matter (see Fig. 16 of Ref. [9]). For the purpose of comparison, we have also deduced temperature of the PNS layer of baryon density of around  $0.63 \times 10^{15} \text{ g/cm}^3$  from our mean-field results (see the last column of Tables II and III), and found that only the CDM3Yn and D1N interactions



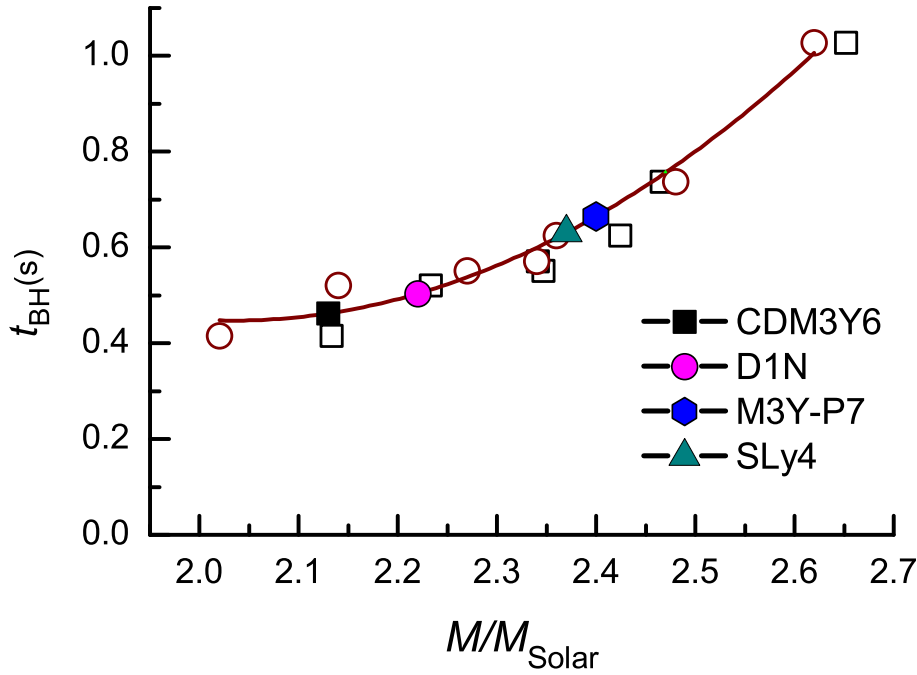


FIG. 27: (Color online) Delay time  $t_{\text{BH}}$  from the onset of the collapse of a  $40 M_{\odot}$  progenitor until the black hole formation as function of the enclosed gravitational mass  $M_{\text{G}}$  (open squares) given by the hydrodynamic simulation [9, 10], and  $M_{\text{max}}$  values given by the solution of the TOV equations using the same EOS for the  $\nu$ -free and  $\beta$ -stable PNS at  $S/A = 4$  (open circles). The  $M_{\text{max}}$  values given by the present mean-field calculation of the  $\nu$ -free and  $\beta$ -stable PNS at  $S/A = 4$  using different density dependent NN interactions are shown on the correlation line interpolated from the results of simulation.

give temperature  $T_s$  in the  $\nu$ -free scenario comparable with that obtained in the hydrodynamic simulation. The temperature  $T_c$  in the center of  $\beta$ -stable hydrostatic PNS given by the CDM3Yn interaction is about 90 and 110 MeV in the  $\nu$ -trapped and  $\nu$ -free scenarios, respectively. The  $T_c$  values given by the D1N, M3Y-P7 and Sly4 interactions are much too high (see Tables III), and this effect is clearly due to the unrealistic behavior of nucleon effective mass predicted by these interactions at high baryon densities (see Figs. 17 and 18). From the above discussion, only the asy-stiff CDM3Yn interaction seems to reproduce the configuration of hot PNS comparable with that given by the hydrodynamic simulation.

We discuss our mean-field results for the  $\nu$ -free and  $\beta$ -stable PNS at  $S/A = 4$  in more details. Because the simulated density profile of temperature reaches its maximum at the total entropy per baryon  $S/A \approx 4$ , the authors of Refs. [9, 10] have compared the stable

hydrostatic configurations obtained with different EOS's for the  $\nu$ -free,  $\beta$ -stable PNS at  $S/A = 4$  with the results of their hydrodynamic simulation. What they found is quite remarkable: the gravitational mass  $M_G$  enclosed inside the shock at the onset of collapse of the  $40 M_\odot$  protoneutron progenitor to black hole (open squares in Fig. 27) given by the simulation is rather close to the maximum gravitational mass  $M_{\max}$  given by the same EOS of hot PNS matter (open circles in Fig. 27). As a result, almost a linear correlation was found between the  $M_{\max}$  value and the delay time  $t_{\text{BH}}$  from the onset of collapse until black hole formation predicted by the simulation [9] (see the solid line in Fig. 27). We have combined, therefore, the results of this interesting study from Refs. [9, 10], and presented the correlation between  $t_{\text{BH}}$ ,  $M_G$  and  $M_{\max}$  values in Fig. 27. Although the  $t_{\text{BH}}$  and  $M_G$  values that might be obtained from the hydrodynamic simulation using the EOS's considered in the present work are still uncertain, we can use the correlation found between  $t_{\text{BH}}$  and  $M_{\max}$  in Refs. [9, 10] to roughly estimate  $t_{\text{BH}}$  based on  $M_{\max}$  values given by the density dependent NN interactions under study. Focusing on the CDM3Y6, Sly4, and M3Y-P7 interactions which give the  $M_{\max}$  value at  $S/A = 0$  close to the observed neutron star mass of around  $1.97 M_\odot$  [58], we find that  $t_{\text{BH}} \approx 0.5$  s might be obtained with the EOS based on the CDM3Y6 interaction, and  $t_{\text{BH}} \approx 0.6 - 0.7$  s with the EOS's based on the Sly4 and M3Y-P7 interactions. These values seem to satisfy the realistic boundary condition  $t_{\text{BH}} \gtrsim 0.5$  s discussed in Ref. [9].

## V. CONCLUSION

A consistent Hartree-Fock calculation of hot asymmetric NM has been performed using several realistic choices of the in-medium density dependent NN interaction, which have been successfully used in nuclear structure and reaction studies. The impact of nuclear symmetry energy and nucleon effective mass to thermal properties of asymmetric NM has been studied in details. We found that the two groups of the interactions (the so-called asy-stiff and asy-soft) that give the stiff and soft behaviors of the symmetry energy of NM at zero temperature also give the same behaviors of the free symmetry energy of hot NM. The free symmetry energy and nucleon effective mass obtained with the asy-stiff CDM3Y3 and CDM3Y6 interactions are in a good agreement with the prediction of the microscopic BHF calculations [12, 52] using the Argonne NN interaction, while those results given by

the asy-soft interactions differ significantly from the BHF results at high NM densities.

We have tested the quadratic approximation for the dependence of the free symmetry energy on the neutron-proton asymmetry  $\delta$  by comparing the results of the HF calculation at different asymmetries  $\delta$ . While this approximation remains reasonable for the internal symmetry energy  $E_{\text{sym}}/A$  at different temperatures, it becomes much poorer for the free symmetry energy  $F_{\text{sym}}/A$  with the increasing temperature. Such a breakdown of the quadratic approximation is due to the contribution of entropy. The HF calculation of hot NM has been done in a fine grid of the baryon number densities, neutron-proton asymmetries, temperatures and entropies to investigate the density profiles of temperature and entropy of hot NM. A very significant impact of the nucleon effective mass  $m^*$  to the thermodynamic properties of hot NM was found, which is directly related to the momentum dependence of the nucleon mean-field potential. At the given baryon density, the smaller the nucleon effective mass the larger the temperature of NM.

The density dependent NN interactions were further used to generate the EOS of baryon matter in the uniform PNS core, which was smoothly connected to the EOS of the inhomogeneous PNS crust by Shen *et al.* [7, 55] for the mean-field study of  $\beta$ -stable PNS matter at finite temperature. Our study considered two different scenarios: the  $\nu$ -trapped matter with the electron lepton fraction  $Y_e \approx 0.4$  and the total entropy per baryon  $S/A = 1, 2$  and 4, which mimics the initial stage of PNS; the  $\nu$ -free matter at  $S/A = 1, 2$  and 4, which is close to the late stage of PNS when most neutrinos have escaped. The impact of nuclear symmetry energy was found significant in the  $\nu$ -free PNS matter where the dynamic neutron-proton asymmetry, baryon and lepton compositions obtained with the asy-stiff and asy-soft interactions are quite different. The high-density behaviors of the density profiles of temperature and entropy of the  $\nu$ -free,  $\beta$ -stable PNS matter are strongly affected not only by the symmetry energy but also by the nucleon effective mass. Although the impact of the symmetry energy was found less significant in the presence of trapped neutrinos, we found that the symmetry energy still affects strongly the neutrino fraction in the  $\nu$ -trapped PNS matter, with  $x_\nu \lesssim 0.1$  given by the asy-stiff interactions at high baryon densities, and  $x_\nu \gtrsim 0.1$  given by the asy-soft interactions.

Using the inputs of the TOV equation based on different EOS's, we obtained the  $\beta$ -stable hydrostatic configuration of PNS at the total entropy per baryon  $S/A = 1, 2$  and 4 in both the  $\nu$ -free and  $\nu$ -trapped scenarios. In the absence of trapped neutrinos, different slopes of

the symmetry energy at high baryon densities were shown to give a difference of  $0.3 - 0.5 M_\odot$  in the maximum gravitational mass  $M_{\text{max}}$  predicted with the CDM3Yn interactions. For the  $\nu$ -trapped,  $\beta$ -stable PNS, the effect of the symmetry energy is diminished already at the entropy  $S/A = 1$  and 2, and the stable values of the maximum gravitational mass and radius of the PNS are rather close, independent of the behavior of the symmetry energy. However, the impact of the nucleon effective mass remains drastic in both  $\nu$ -trapped and  $\nu$ -free cases, with temperature of the PNS matter being inversely proportional to  $m^*$ . In particular, the difference in temperature in both the outer core and center of PNS given by different density dependent NN interactions at  $S/A = 4$  is mainly due to the difference in  $m^*$  because the effect of the symmetry energy is diminished at this high entropy

A special attention was given to the configuration of the  $\nu$ -free PNS at entropy  $S/A = 4$ , which was shown by Hempel *et al.* [9] to occur at the onset of the collapse of a massive ( $40 M_\odot$ ) protoneutron progenitor to black hole. We found that at very high temperatures of PNS matter at  $S/A = 4$ , the impact of the symmetry energy becomes weaker and the similar  $\beta$ -stable configurations of PNS were obtained with both the asy-stiff and asy-soft interactions. The  $M_{\text{max}}$  and  $R_{\text{max}}$  values were found strongly increased at the entropy per baryon  $S/A = 4$ , with the difference  $\Delta M_{\text{max}} \approx 0.3 - 0.5 M_\odot$  and  $\Delta R_{\text{max}} \approx 4 - 5$  km compared to the results obtained at  $S/A = 0$ . Thus, the hot PNS at  $S/A = 4$  is substantially expanded in size, with the decreased central pressure and density. In the outer core of hot PNS being at entropy  $S/A = 4$ , only temperature given by the asy-stiff CDM3Yn interaction is comparable to that predicted by the hydrodynamic simulation. The maximum gravitational masses  $M_{\text{max}}$  obtained for the  $\beta$ -stable and  $\nu$ -free PNS at  $S/A = 4$  using different EOS's of hot NM were used to estimate the time  $t_{\text{BH}}$  of collapse of the  $40 M_\odot$  progenitor to black hole, based on a correlation found between  $t_{\text{BH}}$  and  $M_{\text{max}}$  from the hydrodynamic simulation [9, 10].

In a more general viewpoint, the present mean-field study illustrates the large impact of the nuclear symmetry energy and nucleon effective mass in dense and hot baryon matter. This effect becomes more complicated after the inclusion of trapped neutrinos which weakens the correlation of the thermodynamic properties of PNS with the symmetry energy. The densities and temperatures reached in the core of PNS at entropy of  $S/A \approx 4$  or higher might imply a phase transition to new degrees of freedom as discussed, e.g., in Refs. [62, 63]. Thus, PNS is the most extreme compact object which requires the most advanced knowledge in the nuclear and QCD physics. It is, however, very short-lived because it lasts only a few

minutes before being collapsed to black hole or cooled down to neutron star. Thus, the observation of the next supernova explosion in our galaxy will certainly provide the new and fascinating information about the hot PNS matter that is extremely difficult to obtain in the terrestrial nuclear physics laboratories.

## Acknowledgments

The present research has been supported, in part, by the National Foundation for Scientific and Technological Development (NAFOSTED Project No. 103.04-2014.76), SNCNS project ANR-10-BLAN-0503, and New-Compstar COST action MP1304. N.H.T. is grateful to the University of Lyon for the PALSE incoming mobility fellowship that allowed her short-term stay at Institut de Physique Nucléaire de Lyon (IN2P3-CNRS), to accomplish an important part of this research.

- 
- [1] H.A. Bethe, Rev. Mod. Phys. **62**, 801 (1990).
  - [2] A. Burrows and J.M. Lattimer, Astrophys. J. **307**, 178 (1986).
  - [3] J.M. Lattimer and M. Prakash, Science **304**, 536 (2004).
  - [4] J.M. Lattimer and M. Prakash, Phys. Rep. **442**, 109 (2007).
  - [5] P. Haensel, A.Y. Potekhin, and D.G. Yakovlev, *Neutron Stars 1, Equation of State and Structure*, Astrophysics and Space Science Library, Vol. 326, Springer Science+Business Media, LLC, 2007.
  - [6] S.L. Shapiro and S.A. Teukolsky, *Black Holes, White Dwarfs, and Neutron Stars* (Wiley-VCH Verlag GmbH & Co. KGaA, Weinheim 2004).
  - [7] H. Shen, H. Toki, K. Oyamatsu, and K. Sumiyoshi, Prog. Theor. Phys. **100**, 1013 (1998).
  - [8] D.T. Loan, N.H. Tan, D.T. Khoa, and J. Margueron, Phys. Rev. C **83**, 065809 (2011).
  - [9] M. Hempel, T. Fischer, J. Schaffner-Bielich, and M. Liebendörfer, Astrophys. J. **748**, 70 (2012).
  - [10] A.W. Steiner, M. Hempel, and T. Fischer, Astrophys. J. **774**, 17 (2013).
  - [11] M. Prakash, I. Bombaci, M. Prakash, P.J. Ellis, J.M. Lattimer, and R. Knorren, Phys. Rep. **280**, 1 (1997).

- [12] G.F. Burgio and H.J. Schulze, *Astronomy & Astrophys.* **518**, A17 (2010).
- [13] A. Li, X.R. Zhou, G.F. Burgio, and H.J. Schulze, *Phys. Rev. C* **81**, 025806 (2010).
- [14] F. Douchin and P. Haensel, *Astronomy & Astrophys.*, **380**, 151 (2001).
- [15] T. Klähn *et al.*, *Phys. Rev. C* **74**, 035802 (2006).
- [16] M. Baldo and C. Maieron, *J. Phys. G* **34**, R243 (2007).
- [17] G. Taranto, M. Baldo, and G. F. Burgio, *Phys. Rev. C* **87**, 045803 (2013).
- [18] B.A. Li, L.W. Chen, and C.M. Ko, *Phys. Rep.* **464**, 113 (2008).
- [19] H.S. Than, D.T. Khoa, and N.V. Giai, *Phys. Rev. C* **80**, 064312 (2009).
- [20] G. Bertsch, J. Borysowicz, H. McManus, and W.G. Love, *Nucl. Phys.* **A284**, 399 (1977).
- [21] N. Anantaraman, H. Toki, and G.F. Bertsch, *Nucl. Phys.* **A398**, 269 (1983).
- [22] D.T. Khoa, W. von Oertzen, and A.A. Ogloblin, *Nucl. Phys.* **A602**, 98 (1996).
- [23] D.T. Khoa, G.R. Satchler, and W. von Oertzen, *Phys. Rev. C* **56** (1997) 954.
- [24] D.T. Khoa, H.S. Than, and D.C. Cuong, *Phys. Rev. C* **76**, 014603 (2007).
- [25] D.T. Khoa, W. von Oertzen, H.G. Bohlen, and S. Ohkubo, *J. Phys.* **G34**, R111 (2007).
- [26] H. Nakada, *Phys. Rev. C* **68**, 014316 (2003).
- [27] H. Nakada, *Phys. Rev. C* **78**, 054301 (2008).
- [28] H. Nakada, *Phys. Rev. C* **87**, 014336 (2013).
- [29] J.F. Berger, M. Girod, and D. Gogny, *Comp. Phys. Comm.* **63**, 365 (1991).
- [30] F. Chappert, M. Girod, and S. Hilaire, *Phys. Lett. B* **668**, 420 (2008).
- [31] E. Chabanat, P. Bonche, P. Haensel, J. Meyer, and R. Schaeffer, *Nucl. Phys.* **A627**, 710 (1997).
- [32] E. Chabanat, P. Bonche, P. Haensel, J. Meyer, and R. Schaeffer, *Nucl. Phys.* **A635**, 231 (1998).
- [33] C. Constantinou, B. Muccioli, M. Prakash, and J.M. Lattimer, *Phys. Rev. C* **89**, 065802 (2014).
- [34] C. Wellenhofer, J.W. Holt, and N. Kaiser, *Phys. Rev. C* **92**, 015801 (2015).
- [35] C. Constantinou, B. Muccioli, M. Prakash, and J.M. Lattimer, *Phys. Rev. C* **92**, 025801 (2015).
- [36] A. Fedoseew and H. Lenske, *Phys. Rev. C* **91**, 034307 (2015).
- [37] M. Hempel, *Phys. Rev. C* **91**, 055807 (2015).
- [38] N.M. Hugenholtz and L. Van Hove, *Physica* **24**, 363 (1958).

- [39] D.T. Loan, B.M. Loc, and D.T. Khoa, Phys. Rev. C **92**, 034304 (2015).
- [40] M.B. Tsang, Y. Zhang, P. Danielewicz, M. Famiano, Z. Li, W.G. Lynch, and A.W. Steiner, Phys. Rev. Lett. **102**, 122701 (2009).
- [41] J. Piekarewicz and M. Centelles, Phys. Rev. C **79**, 054311 (2009).
- [42] T. Li *et al.*, Phys. Rev. Lett. **99**, 162503 (2007).
- [43] *Topical Issue on Nuclear Symmetry Energy*, edited by B.A. Li, A. Ramos, G. Verde, and I. Vidaña, Eur. Phys. J. A **50**, No.2, (2014).
- [44] G. Colò, U. Garg, and H. Sagawa, Eur. Phys. J. A **50**, 26 (2014).
- [45] C. Xu, B.A. Li, and L.W. Chen, Eur. Phys. J. A **50**, 21 (2014).
- [46] B.A. Li and X. Han, Phys. Lett. B **727**, 276 (2013).
- [47] D.T. Khoa, B.M. Loc, and D.N. Thang, Eur. Phys. J. A **50**, 34 (2014).
- [48] J.P. Jeukenne, A. Lejeune and C. Mahaux, Phys. Rev. C **16**, 80 (1977).
- [49] A. Lejeune, Phys. Rev. C **21**, 1107 (1980).
- [50] P.E. Hodgson, Contemp. Phys. **24**, 491 (1983).
- [51] R.B. Wiringa, V.G.J. Stoks, and R. Schiavilla, Phys. Rev. C **51**, 38 (1995).
- [52] M. Baldo, G.F. Burgio, H.J. Schulze, and G. Taranto, Phys. Rev. C **89**, 048801 (2014).
- [53] B.A. Li and L.W. Chen, Modern Physics Letters A **30**, 1530010 (2015).
- [54] A.W. Steiner, M. Prakash, and J.M. Lattimer, Phys. Lett. B **486**, 239 (2000).
- [55] <http://user.numazu-ct.ac.jp/~sumi/eos/index.html>
- [56] J. Xu, L.W. Chen, C.M. Ko, and B.A. Li, Phys. Rev. C **81**, 055805 (2010).
- [57] I. Vidaña, I. Bombaci, A. Polls, and A. Ramos, Astronomy & Astrophys., **399**, 687 (2003).
- [58] P.B. Demorest, T. Pennucci, S.M. Ransom, M.S.E. Roberts, and J.W.T. Hessels, Nature, 467, 1081 (2010).
- [59] T. Fisher, S.C. Whitehouse, A. Mezzacappa, F.K. Thielemann, and M. Liebendörfer, Astronomy & Astrophys., **499**, 1 (2009).
- [60] J.M. Lattimer, C.J. Pethick, M. Prakash, and P. Haensel, Phys. Rev. Lett. **66**, 22 (1991).
- [61] K. Kotake, K. Sato, and K. Takahashi, Rep. Prog. Phys. **69**, 971 (2006)
- [62] M. Oertel, A. F. Fantina, and J. Novak Phys. Rev. C **85**, 055806 (2012).
- [63] J. A. Pons, S. Reddy, P. J. Ellis, M. Prakash, and J. M. Lattimer, Phys. Rev. C **62**, 035803 (2000).

## Appendix A: Explicit HF expressions obtained with the finite-range CDM3Yn, M3Y-Pn, and Gogny interactions

For the interested readers who might want to reconstruct various nuclear EOS's used in the present mean-field study, we give in this appendix the explicit presentation of the density dependent NN interactions used in the HF calculation of NM. In general, the (central) NN interaction can be given in terms of the spin- and isospin dependent, direct (D) and exchange (EX) components as

$$v_{\text{D(EX)}}(r) = v_{00}^{\text{D(EX)}}(r) + v_{10}^{\text{D(EX)}}(r)\boldsymbol{\sigma}_1 \cdot \boldsymbol{\sigma}_2 + v_{01}^{\text{D(EX)}}(r)\boldsymbol{\tau}_1 \cdot \boldsymbol{\tau}_2 + v_{11}^{\text{D(EX)}}(r)(\boldsymbol{\sigma}_1 \cdot \boldsymbol{\sigma}_2)(\boldsymbol{\tau}_1 \cdot \boldsymbol{\tau}_2), \quad (\text{A1})$$

where  $\boldsymbol{\sigma}$  and  $\boldsymbol{\tau}$  are the Pauli spin and isospin operators, respectively. Except of the Sly4 interaction, the CDM3Yn, M3Y-Pn, and Gogny interactions are of *finite-range*. For the spin-saturated NM, only the spin-independent ( $v_{00}$  and  $v_{01}$ ) components of the central NN interaction are needed in the HF calculation of NM, because the contributions of the spin-dependent terms in Eq. (A1) to the NM energy are averaged out.

Thus, the density dependent CDM3Yn interaction was used in the present HF calculation explicitly as

$$v_{\text{D(EX)}}(n_b, r) = F_0(n_b)v_{00}^{\text{D(EX)}}(r) + F_1(n_b)v_{01}^{\text{D(EX)}}(r)\boldsymbol{\tau}_1 \cdot \boldsymbol{\tau}_2, \text{ where } r = |\mathbf{r}_1 - \mathbf{r}_2|. \quad (\text{A2})$$

The radial parts  $v_{00(01)}^{\text{D(EX)}}(r)$  are kept unchanged as determined from the M3Y-Paris interaction [21], in terms of three Yukawas

$$v_{00(01)}^{\text{D(EX)}}(r) = \sum_{k=1}^3 Y_{00(01)}^{\text{D(EX)}}(k) \frac{\exp(-a_k r)}{a_k r}. \quad (\text{A3})$$

The density dependence of the CDM3Yn interaction (A2) was assumed to have the same functional form as that introduced first in Ref. [23]

$$F_{0(1)}(n_b) = C_{0(1)}[1 + \alpha_{0(1)} \exp(-\beta_{0(1)} n_b) + \gamma_{0(1)} n_b]. \quad (\text{A4})$$

The parameters of the IS density dependence  $F_0(n_b)$  were determined [23] to reproduce the saturation properties of symmetric NM and give the nuclear incompressibility  $K = 218$  and 252 MeV with the CDM3Y3 and CDM3Y6 versions, respectively. The parameters of the IV density dependence  $F_1(n_b)$  were determined [39] to consistently reproduce the BHF results for the nucleon OP in asymmetric NM [48, 49] in the HF calculation as well as the measured



charge-exchange ( $p, n$ ) and ( ${}^3\text{He}, t$ ) data for the isobar analog states in the folding model (coupled-channel) analysis [24, 47]. The ranges and strengths of Yukawa functions and parameters of the density dependence  $F_{0(1)}(n_b)$  are given in Tables IV and V, respectively. For the soft version CDM3Yns of the CDM3Yn interaction, the IV density dependence was assumed in the same functional form as that of the IS density dependence, with the strength slightly scaled,  $F_1(n_b) \approx 1.1F_0(n_b)$ , to obtain the same symmetry energy  $\varepsilon_{\text{sym}} \approx 32$  MeV at the saturation density  $n_0$  in the HF calculation [8, 22].

As variance with the CDM3Yn interaction, the density dependence of the M3Y-Pn and Gogny interactions are introduced via a *zero-range* density dependent term

$$v_{00(01)}^{\text{D(EX)}}(n_b, r) = v_{00(01)}^{\text{D(EX)}}(r) + d_{00(01)}^{\text{D(EX)}}(n_b, r). \quad (\text{A5})$$

The first term of the M3Y-Pn interaction (A5) has the same finite-range form as that given in Eq. (A3), with the Yukawa ranges and strengths given in Table IV. The direct and exchange parts of the density dependent term  $d_{00(01)}(n_b, r)$  of the M3Y-Pn interaction are the same and can be given explicitly in terms of single-even (SE) and triplet-even (TE) components of the two-nucleon force as

$$\begin{aligned} d_{00}^{\text{D}}(n_b, r) &= d_{00}^{\text{EX}}(n_b, r) = \frac{3}{8} (t_{\text{SE}} n_b + t_{\text{TE}} n_b^{1/3}) \delta(\mathbf{r}), \\ d_{01}^{\text{D}}(n_b, r) &= d_{01}^{\text{EX}}(n_b, r) = \frac{1}{8} (t_{\text{SE}} n_b - 3t_{\text{TE}} n_b^{1/3}) \delta(\mathbf{r}), \end{aligned} \quad (\text{A6})$$

with  $t_{\text{SE}} = 830$  MeV fm<sup>6</sup> and  $t_{\text{TE}} = 1478$  MeV fm<sup>4</sup> adopted for the M3Y-P7 version [28].

The finite-range part of Gogny interaction is similar to that of the M3Y-Pn interaction, but with the radial dependence parametrized in terms of two Gaussians

$$v_{00(01)}^{\text{D(EX)}}(r) = \sum_{k=1}^2 G_{00(01)}^{\text{D(EX)}}(k) \exp\left(-\frac{r^2}{b_k^2}\right), \quad (\text{A7})$$

where Gaussian ranges and strengths used with the D1N version are given in Table IV. The direct and exchange parts of the density dependent term  $d_{00(01)}(n_b, r)$  of Gogny interaction can be explicitly given as

$$\begin{aligned} d_{00}^{\text{D}}(n_b, r) &= \frac{t_0}{2} (2 + x_0) n_b^{1/3} \delta(\mathbf{r}), \quad d_{01}^{\text{D}}(n_b, r) = 0; \\ d_{00}^{\text{EX}}(n_b, r) &= d_{01}^{\text{EX}}(n_b, r) = -\frac{t_0}{4} (1 + 2x_0) n_b^{1/3} \delta(\mathbf{r}), \end{aligned} \quad (\text{A8})$$

with  $t_0 = 1609.46$  MeV fm<sup>4</sup> and  $x_0 = 1$  adopted for the D1N version [30].

TABLE IV: Ranges and strengths of Yukawa and Gaussian functions used in the radial dependence of the M3Y-Paris, M3Y-P7, and D1N interactions.

Interaction	$k$	$a_k$ (fm $^{-1}$ )	$Y_{00}^D(k)$ (MeV)	$Y_{01}^D(k)$ (MeV)	$Y_{00}^{\text{EX}}(k)$ (MeV)	$Y_{01}^{\text{EX}}(k)$ (MeV)	Reference
M3Y-Paris	1	4.0	11061.625	313.625	-1524.25	-4118.0	[21]
	2	2.5	-2537.5	223.5	-518.75	1054.75	
	3	0.7072	0.0	0.0	-7.8474	2.6157	
M3Y-P7	1	4.0	12113.375	680.625	-4520.75	-2945.75	[28]
	2	2.5	-2467.188	219.188	-589.063	1059.063	
	3	0.7072	0.0	0.0	-7.8474	2.6157	
D1N	$k$	$b_k$ (fm)	$G_{00}^D(k)$ (MeV)	$G_{01}^D(k)$ (MeV)	$G_{00}^{\text{EX}}(k)$ (MeV)	$G_{01}^{\text{EX}}(k)$ (MeV)	[30]
	1	0.8	-369.673	827.628	-26.290	-338.175	
	2	1.2	14.545	-128.085	-32.410	77.135	

TABLE V: Parameters of the density dependence (A4) of the CDM3Yn interaction

Interaction	$i$	$C_i$	$\alpha_i$	$\beta_i$ (fm $^3$ )	$\gamma_i$ (fm $^3$ )	Reference
CDM3Y3	0	0.2985	3.4528	2.6388	-1.500	[23]
	1	0.2343	7.6514	9.7494	6.6317	[39]
CDM3Y6	0	0.2658	3.8033	1.4099	-4.000	[23]
	1	0.2313	7.6800	9.6498	6.7202	[39]

Dividing the total energy density (1) of NM over the corresponding baryon number density  $n_b$ , one obtains the internal NM energy per particle with the CDM3Yn, M3Y-Pn, and Gogny interactions as

$$\frac{E}{A}(T, n_b, \delta) = \mathcal{E}_{\text{kin}}(T, n_b, \delta) + \mathcal{E}_{\text{pot}}(T, n_b, \delta), \quad (\text{A9})$$

$$\begin{aligned}
\text{where } \mathcal{E}_{\text{kin}}(T, n_b, \delta) &= \frac{2}{(2\pi)^3 n_b} \sum_{\tau=n,p} \frac{\hbar^2}{2m_\tau} \int n_\tau(\mathbf{k}, T) k^2 d\mathbf{k}; \\
\mathcal{E}_{\text{pot}}(T, n_b, \delta) &= \mathcal{E}_{\text{IS}}(T, n_b, \delta) + \mathcal{E}_{\text{IV}}(T, n_b, \delta), \\
\mathcal{E}_{\text{IS(IV)}}(T, n_b, \delta) &= \mathcal{E}_{\text{IS(IV)}}^{\text{D}}(n_b, \delta) + \mathcal{E}_{\text{IS(IV)}}^{\text{EX}}(T, n_b, \delta).
\end{aligned} \tag{A10}$$

It is noteworthy that at finite temperature the kinetic energy term is affected by different EOS's via the single-particle potential embedded in the nucleon momentum distribution  $n_\tau(\mathbf{k}, T)$ . The *direct* term of the (isoscalar and isovector) potential energy is obtained compactly with the CDM3Yn interaction as

$$\mathcal{E}_{\text{IS}}^{\text{D}}(n_b) = \frac{n_b}{2} F_0(n_b) J_0^D, \quad \mathcal{E}_{\text{IV}}^{\text{D}}(n_b) = \delta^2 \frac{n_b}{2} F_1(n_b) J_1^D, \tag{A11}$$

where  $J_{0(1)}^{\text{D}} = \int v_{00(01)}^{\text{D}}(r) d\mathbf{r}$ . The corresponding *exchange* term can be obtained with the CDM3Yn interaction in the following integral form

$$\begin{aligned}
\mathcal{E}_{\text{IS}}^{\text{EX}}(T, n_b, \delta) &= \frac{F_0(n_b)}{8n_b\pi^5} \int n_b(\mathbf{k}, T) H_{\text{IS}}(n_b, \mathbf{k}, \delta, T) d\mathbf{k}, \\
\mathcal{E}_{\text{IV}}^{\text{EX}}(T, n_b, \delta) &= \frac{F_1(n_b)}{8n_b\pi^5} \int \Delta n_b(\mathbf{k}, T) H_{\text{IV}}(n_b, \mathbf{k}, \delta, T) d\mathbf{k}.
\end{aligned} \tag{A12}$$

Here  $n_b(\mathbf{k}, T) = n_n(\mathbf{k}, T) + n_p(\mathbf{k}, T)$ ,  $\Delta n_b(\mathbf{k}, T) = n_n(\mathbf{k}, T) - n_p(\mathbf{k}, T)$ , and

$$\begin{aligned}
H_{\text{IS}}(n_b, \mathbf{k}, \delta, T) &= \int n_b(\mathbf{k}', T) d\mathbf{k}' \int_0^\infty j_0(kr) j_0(k'r) v_{00}^{\text{EX}}(r) r^2 dr, \\
H_{\text{IV}}(n_b, \mathbf{k}, \delta, T) &= \int \Delta n_b(\mathbf{k}', T) d\mathbf{k}' \int_0^\infty j_0(kr) j_0(k'r) v_{01}^{\text{EX}}(r) r^2 dr.
\end{aligned} \tag{A13}$$

Note that the direct term of the potential energy is the same as that obtained at zero temperature [8, 22], and the explicit temperature dependence is embedded entirely in the exchange (Fock) term. Thus, a proper treatment of Pauli blocking in the mean-field studies of hot NM is indeed very important.

The exchange term of the potential energy given by the finite-range, density independent part of the M3Y-Pn and Gogny interactions can be obtained in the same expression (A12), but with  $F_{0(1)}(n_b) = 1$ . It is convenient to include the contribution from the zero-range, density dependent part of these interactions into the direct term of the potential energy

$$\mathcal{E}_{\text{IS}}^{\text{D}}(n_b) = \frac{n_b}{2} [J_0^D + D_{\text{IS}}(n_b)], \quad \mathcal{E}_{\text{IV}}^{\text{D}}(n_b) = \delta^2 \frac{n_b}{2} [J_1^D + D_{\text{IV}}(n_b)], \tag{A14}$$

where  $D_{\text{IS(IV)}}(n_b)$  are given explicitly by the M3Y-Pn interaction as

$$D_{\text{IS}}(n_b) = \frac{3}{4} (t_{\text{SE}} n_b + t_{\text{TE}} n_b^{1/3}), \quad D_{\text{IV}}(n_b) = \frac{1}{4} (t_{\text{SE}} n_b - 3t_{\text{TE}} n_b^{1/3}), \tag{A15}$$

and by Gogny interaction as

$$D_{\text{IS}}(n_b) = \frac{3}{4}t_0n_b^{1/3}, \quad D_{\text{IV}}(n_b) = -\frac{t_0}{4}(1+2x_0)n_b^{1/3}. \quad (\text{A16})$$

The momentum- and density dependent single-particle potential (9)-(10) can be expressed in terms of the IS and IV parts as

$$U_\tau(n_b, \mathbf{k}, \delta, T) = U_{\text{IS}}^{(\text{HF})}(n_b, \mathbf{k}, \delta, T) \pm U_{\text{IV}}^{(\text{HF})}(n_b, \mathbf{k}, \delta, T) + U_{\text{IS}}^{(\text{RT})}(n_b, \delta, T) + U_{\text{IV}}^{(\text{RT})}(n_b, \delta, T) \quad (\text{A17})$$

where the sign + pertains to neutron and - to proton, and

$$U_{\text{IS(IV)}}^{(\text{HF})}(n_b, \mathbf{k}, \delta, T) = U_{\text{IS(IV)}}^{\text{D}}(n_b, \delta) + U_{\text{IS(IV)}}^{\text{EX}}(n_b, \mathbf{k}, \delta, T) \quad (\text{A18})$$

The *direct* term of the (IS and IV) HF potential is given by the CDM3Yn interaction as

$$U_{\text{IS}}^{\text{D}}(n_b) = n_b F_0(n_b) J_0^{\text{D}}, \quad U_{\text{IV}}^{\text{D}}(n_b, \delta) = n_b F_1(n_b) J_1^{\text{D}} \delta. \quad (\text{A19})$$

The corresponding *exchange* exchange term of the HF potential is given by the CDM3Yn interaction as

$$U_{\text{IS(IV)}}^{\text{EX}}(n_b, \mathbf{k}, \delta, T) = \frac{F_{0(1)}(n_b)}{\pi^2} H_{\text{IS(IV)}}(n_b, \mathbf{k}, \delta, T). \quad (\text{A20})$$

The rearrangement term of the single-particle potential (A17) is obtained in terms of its direct and exchange terms, and one has in case of the CDM3Yn interaction

$$\begin{aligned} U_{\text{IS}}^{(\text{RT})}(n_b, \delta, T) &= \frac{\partial F_0(n_b)}{\partial n_b} \left[ \frac{n_b^2}{2} J_0^{\text{D}} + \frac{1}{8\pi^5} \int n_b(\mathbf{k}, T) H_{\text{IS}}(n_b, \mathbf{k}, \delta, T) d\mathbf{k} \right], \\ U_{\text{IV}}^{(\text{RT})}(n_b, \delta, T) &= \frac{\partial F_1(n_b)}{\partial n_b} \left[ \delta^2 \frac{n_b^2}{2} J_1^{\text{D}} + \frac{1}{8\pi^5} \int \Delta n_b(\mathbf{k}, T) H_{\text{IV}}(n_b, \mathbf{k}, \delta, T) d\mathbf{k} \right]. \end{aligned} \quad (\text{A21})$$

One can see that the explicit temperature dependence of single-particle potential is entirely embedded in the exchange terms of  $U^{(\text{HF})}$  and  $U^{(\text{RT})}$ . Moreover, the explicit momentum dependence of single-particle potential (needed for the estimation of the nucleon effective mass) is also contained in the exchange term of the HF potential (A20) only. All this indicates the vital role of Pauli blocking in dense NM.

The exchange term of the HF potential given by the finite-range, density independent part of the M3Y-Pn and Gogny interactions can be obtained in the same expression (A20), but with  $F_{0(1)}(n_b) = 1$ . It is also convenient to include the contribution from the zero-range (density dependent) part of these interactions into the direct part of the HF potential as

$$U_{\text{IS}}^{\text{D}}(n_b) = n_b [J_0^{\text{D}} + D_{\text{IS}}(n_b)], \quad U_{\text{IV}}^{\text{D}}(n_b, \delta) = n_b \delta [J_1^{\text{D}} + D_{\text{IV}}(n_b)]. \quad (\text{A22})$$

As variance with the CDM3Yn case, the rearrangement term of single particle potential given by the M3Y-Pn interaction does not depend on temperature

$$U_{\text{IS}}^{(\text{RT})}(n_b) = \frac{3}{8}(t_{\text{SE}}n_b^2 + \frac{1}{3}t_{\text{TE}}n_b^{4/3}), \quad U_{\text{IV}}^{(\text{RT})}(n_b, \delta) = \frac{\delta^2}{8}(t_{\text{SE}}n_b^2 - t_{\text{TE}}n_b^{4/3}). \quad (\text{A23})$$

Likewise, the (temperature independent) rearrangement term of single particle potential is given by Gogny interaction as

$$U_{\text{IS}}^{(\text{RT})}(n_b) = \frac{1}{8}t_0n_b^{4/3}, \quad U_{\text{IV}}^{(\text{RT})}(n_b, \delta) = -\delta^2\frac{t_0}{24}(1 + 2x_0)n_b^{4/3}. \quad (\text{A24})$$

The density- and temperature dependent nucleon effective mass (22) can be explicitly obtained with the CDM3Yn interaction using Eq. (A20)

$$\begin{aligned} \frac{m_\tau^*(n_b, \delta, T)}{m} = & \left\{ 1 - \frac{m}{\hbar^2\pi^2k_F^\tau} \left[ F_0(n_b) \int_0^\infty j_1(kr)v_{00}^{\text{EX}}(r)r^3dr \int n_b(\mathbf{k}', T)j_0(k'r)d\mathbf{k}' \right. \right. \\ & \left. \pm F_1(n_b) \int_0^\infty j_1(kr)v_{01}^{\text{EX}}(r)r^3dr \int \Delta n_b(\mathbf{k}', T)j_0(k'r)d\mathbf{k}' \right] \right\}^{-1}, \end{aligned} \quad (\text{A25})$$

where  $j_1(x)$  is the first-order spherical Bessel function, and the + sign pertains to neutron and - to proton. The nucleon effective mass in hot NM given by the M3Y-Pn and Gogny interactions can be obtained in the same expression (A25), but with  $F_{0(1)}(n_b) = 1$ . We emphasize again that the nuclear medium modification responsible for the nucleon effective mass is fully given by the exchange (Fock) term of single-particle potential.

## Appendix B: Explicit HF expressions obtained with the zero-range Skyrme interaction

The central zero-range Skyrme interaction [31, 32] has been used in the present HF calculation explicitly as

$$\begin{aligned} v(\mathbf{r}) = & t_0(1 + x_0P_\sigma)\delta(\mathbf{r}) + \frac{t_1}{2}(1 + x_1P_\sigma)[\overleftarrow{\mathbf{P}}^2\delta(\mathbf{r}) + \delta(\mathbf{r})\overrightarrow{\mathbf{P}}^2] \\ & + t_2(1 + x_2P_\sigma)(\overleftarrow{\mathbf{P}} \cdot \delta(\mathbf{r})\overrightarrow{\mathbf{P}}) + \frac{t_3}{6}(1 + x_3P_\sigma)[n_b(\mathbf{R})]^\gamma\delta(\mathbf{r}). \end{aligned} \quad (\text{B1})$$

Here  $\mathbf{r} = \mathbf{r}_1 - \mathbf{r}_2$ ,  $\mathbf{R} = \frac{1}{2}(\mathbf{r}_1 + \mathbf{r}_2)$ ,  $\overrightarrow{\mathbf{P}} = \frac{1}{2i}(\overrightarrow{\nabla}_1 - \overrightarrow{\nabla}_2)$ , and  $\overleftarrow{\mathbf{P}} = \frac{1}{2i}(\overleftarrow{\nabla}_1 - \overleftarrow{\nabla}_2)$ . The spin exchange operator in Eq. (B1) is taken as  $P_\sigma = -P_\tau P_r$ , where  $P_\tau$  and  $P_r$  apply the exchange of isospins ( $\tau_1 \rightleftharpoons \tau_2$ ) and spacial coordinates ( $\mathbf{r}_1 \rightleftharpoons \mathbf{r}_2$ ), respectively.

Instead of (A9), the internal NM energy per particle is obtained explicitly with Skyrme interaction as

$$\begin{aligned} \frac{E}{A}(T, n_n, n_p) = & \mathcal{E}_{\text{kin}}(T, n_n, n_p) + \frac{t_0}{4n_b}[(2+x_0)n_b^2 - (2x_0+1)(n_p^2 + n_n^2)] \\ & + \frac{t_3}{24}n_b^{\gamma-1}[(2+x_3)n_b^2 - (2x_3+1)(n_p^2 + n_n^2)], \end{aligned} \quad (\text{B2})$$

$$\text{where } \mathcal{E}_{\text{kin}}(T, n_n, n_p) = \frac{1}{n_b} \sum_{\tau=n,p} \frac{\hbar^2 \mathcal{K}_\tau(T)}{2m_\tau^*}, \text{ with } \mathcal{K}_\tau(T) = \frac{2}{(2\pi)^3} \int n_\tau(\mathbf{k}, T) k^2 d\mathbf{k}. \quad (\text{B3})$$

Due to the zero range of Skyrme interaction, the temperature dependence implied by the nucleon momentum distribution is integrated out and the potential energy term in Eq. (B2) turns out to be the same as that at zero temperature. As a result, the temperature dependence of the internal NM energy is entirely embedded in the kinetic energy term (B3), where the (temperature independent) nucleon effective mass  $m_\tau^*$  is determined as

$$\begin{aligned} \frac{m_\tau^*(n_n, n_p)}{m} = & \left[ 1 + \frac{m}{4\hbar^2}(\Theta_1 n_b + \Theta_2 n_\tau) \right]^{-1}, \\ \text{with } \Theta_1 = & t_1(2+x_1) + t_2(2+x_2), \\ \Theta_2 = & t_2(2x_2+1) - t_1(2x_1+1). \end{aligned} \quad (\text{B4})$$

The momentum- and density dependent single-particle potential (9)-(10) can be obtained with Skymre interaction explicitly as

$$\begin{aligned} U_\tau(n_n, n_p, \mathbf{k}, T) = & U_\tau^{(\text{HF})}(n_n, n_p, \mathbf{k}, T) + U^{(\text{RT})}(n_n, n_p), \\ U_\tau^{(\text{HF})}(n_n, n_p, \mathbf{k}, T) = & \frac{t_0}{2}[(2+x_0)n_b - (2x_0+1)n_\tau] + \Theta_1[\mathcal{K}_n(T) + \mathcal{K}_p(T)] + \Theta_2 \mathcal{K}_\tau(T) \\ & + \frac{t_3}{12}n_b^\gamma[(2+x_3)n_b - (2x_3+1)n_\tau] + \frac{1}{8}[\Theta_1 n_b + \Theta_2 n_\tau] \mathbf{k}^2, \end{aligned} \quad (\text{B5})$$

$$\text{and } U^{(\text{RT})}(n_n, n_p) = \frac{t_3}{24}n_b^{\gamma-1}[(2+x_3)n_b^2 - (2x_3+1)(n_n^2 + n_p^2)]. \quad (\text{B6})$$

Like the potential energy term in Eq. (B2), the temperature dependence of single particle potential is also given by that of the kinetic energy term, via  $\mathcal{K}_\tau(T)$  values. With the explicit momentum dependence of Skyrme interaction (B1), the HF term of single-particle potential (B5) has a quadratic momentum dependence that gives the nucleon effective mass (B4). Like the case of M3Y-Pn and Gogny interactions, the rearrangement term (B6) of Skyrme single-particle potential is also temperature independent.

The explicit parameters of the SLy4 version [32] of Skyrme interaction used in the present HF calculation are:  $t_0=-2488.91 \text{ MeV fm}^3$ ,  $t_1=486.82 \text{ MeV fm}^5$ ,  $t_2=-546.39 \text{ MeV fm}^5$ ,  $t_3=13777.0 \text{ MeV fm}^{3+3\gamma}$ ,  $x_0=0.834$ ,  $x_1=-0.344$ ,  $x_2=-1.000$ ,  $x_3=1.354$ , and  $\gamma = 1/6$ .